KINETICS OF AN INVERSE TEMPERATURE TRANSITION PROCESS AND ITS APPLICATION ON SUPPORTED LIPID BILAYERS

A Dissertation

by

CHIN-YUAN CHANG

Submitted to the Office of Graduate Studies of
Texas A&M University
in partial fulfillment of the requirements for the degree of

DOCTOR OF PHILOSOPHY

August 2010

Major Subject: Chemistry

Kinetics of an Inverse Temperature Transition Process and Its Application on Supported Lipid Bilayers

KINETICS OF AN INVERSE TEMPERATURE TRANSITION PROCESS AND ITS APPLICATION ON SUPPORTED LIPID BILAYERS

A Dissertation

by

CHIN-YUAN CHANG

Submitted to the Office of Graduate Studies of
Texas A&M University
in partial fulfillment of the requirements for the degree of

DOCTOR OF PHILOSOPHY

Approved by:

Chair of Committee,	Paul S. Cremer
Committee Members,	James D. Batteas
	J. Martin Scholtz
	Emile A. Schweikert
Head of Department,	David H. Russell

August 2010

Major Subject: Chemistry

ABSTRACT

Kinetics of an Inverse Temperature Transition Process and Its Application on Supported Lipid Bilayers. (August 2010)

Chin-Yuan Chang, B.S.; M.S., National Taiwan University, Taiwan

Chair of Advisory Committee: Dr. Paul S. Cremer

This dissertation focuses on the study of inverse temperature transition processes of the poly(*N*-isopropylacrylamide) (PNIPAM) and the elastin-like polypeptides (ELPs). A novel temperature jump microfluidic system is introduced and this system shows the ability to measure the kinetics of the PNIPAM and the ELPs collapse without a heat transfer problem. The conformational change of the ELPs during the phase transition process is utilized as a nanoscale protein filter to modulate ligand-receptor binding events on supported lipid bilayers (SLBs).

This research study is divided into three main parts. The first part is the development of the temperature jump microfluidics. The kinetics of PNIPAM collapse is used as a model system to show the capability of this new device to measure millisecond time scale phase transition processes. The effects of salts on the kinetics of PNIPAM collapse are also shown in this part. To our knowledge, this is the first study which shows the effects of salts on PNIPAM collapse kinetics.

The second part of this research is the application of the novel temperature jump microfluidics. The hydrophobic collapse of ELPs composed of identical sequence but different chain length is investigated. By controlling the molecular weight of the ELPs,

the thermodynamic contributions from intermolecular hydrophobic interactions, and intramolecular hydrophobic interactions could be calculated individually for this unique system.

The third part is the application of the phase transition property of ELPs. The ELPs are conjugated on the surface of the SLBs as a nanoscale protein filter. The conformation of the ELPs can be modulated by ionic strength of the buffer solution or ambient temperature. The ELPs conjugated SLBs platform showed the ability to block IgG binding to biotin conjugated on the SLBs when the ELPs were in the extended coil state and open the access for protein to bind to biotin in compact globule conformation.

DEDICATION

To my parents, Cheng-Liang Chang and Su-chin Lu

and

to my wife, Hsin-Ya Liu

and

to my daughter, Lucia F. Chang

ACKNOWLEDGEMENTS

First of all, I would like to give thanks to my advisor, Dr. Paul S. Cremer, for his guidance, support and patience throughout my study at Texas A&M University. I was very lucky to join his research group and have the chance to do research in a free environment under his advice. I would also like to thank Dr. Hilty, Dr. Scholtz and Dr. Batteas for serving as my committee members and for their guidance and helpful advice.

I sincerely thank my fellow Cremer group members and friends for their support and help during these years and for providing a unique and fun work atmosphere. I especially thank Dr. Yanjie Zhang, Dr. Tinglu Yang, Dr. Laura Sagle, Younhee, Jaibir and Aaron for the helpful discussions and dedication to my research; Dr. Monson, Dr. Heck, Dr. Piramuthu, Dr. Cai, Jixin, Sarah, Sean, Chunming, Hudson, George, Da, Halil, Kelvin, Qian and Jennifer for the great experience working with them. I would also like to thank my advisor, Dr. Chuen-Ying Liu, in National Taiwan University for encouraging me to study abroad and the Liu group for the help in the past.

Finally, I would like to thank my family, my wife, Hsin-Ya, for the love, support, understanding and patience in all these years being with me, my daughter, Lucia, for giving me strength to carry on, and my parents and sister in Taiwan for the love, support, understanding and sacrifices for all those years. I can not do anything without the love from my family.

Financial support from National Science Foundation (CHE-0809854) and The Robert A. Welch Foundation (A-1421) are also acknowledged.

TABLE OF CONTENTS

CHAPTER Page

LIST OF FIGURES

FIGURE Page

FIGURE Page

FIGURE Page

LIST OF TABLES

CHAPTER I

INTRODUCTION

1.1 Purpose/Objective

The dynamics of the protein folding from a denatured random coil state to a native globule state in which it possess activity[1] is not well understood.[2-3] Studying the pathway and the mechanism of the protein folding may provide more information to know the structures and the functions of thousands of protein sequences.[4] On the other hand, the understanding of the cold denaturation is far less compare to heat denaturation due to the fact that cold denaturation always occurs below freezing temperature of water and it is hard to study in aqueous solution.[5] The study of the homopolymer chains collapse from extended random coils to compact globule states (coil-to-globule transition) may provide more understanding of initial stage of protein folding.[1,6]

Though the coil-to-globule transition in poor solvents is a much simpler model to study the protein folding process, this phase transition process is still not well studied as well.[6] It is difficult to study this kind of kinetic process especially when it is triggered by temperature change. Some attempts have been made by measuring the radius change during collapse by the dynamic laser light scattering,[7-9] but the heat transfer efficiency was always a problem in this kind of experiment.

This dissertation follows the style of *Journal of the American Chemical Society.*

The study reported in this dissertation is focus on the development of a novel temperature-jump microfluidic device to study the kinetics of phase transition processes of a temperature-responsive polymer, poly(*N*-isopropylacrylamide) (PNIPAM), and elastin-like polypeptides (ELPs) under different conditions such as in the presence of different salts and the effects of chain length. Microfluidic device was employed to overcome the heat transfer problem by reducing sample volume, increasing heating area and also providing preheated channels prior to sample introduction. By utilizing PNIPAM and ELPs as model systems, we are able to study the kinetics of hydrophobic collapse under different conditions which are related to the protein folding and also obtain thermodynamic parameters by fitting kinetic parameters to a transition state theory[10].

The applications of ELPs on solid supported lipid bilayers (SLBs) also have been shown in this dissertation. ELPs conjugated SLBs are presented as a platform showing the ability to modulate the ligand-receptor binding by changing ionic strength of buffers or ambient temperatures. Previously, a SLBs microfluidic platform was made with lipopolymer, poly(ethylene glycol)[11] (PEG) so that the conformation of the PEG is controlled by its density on the bilayer surface. In low density, the PEG is in mushroom conformation so the IgG in bulk solution can access the biotin on the membrane surface. As density of the PEG goes higher than the transition density, the PEG undergoes a mushroom-to-brush transition and the access of IgG to biotin will be blocked by the brush-like PEG on bilayer surface. An advanced design is presented here that the conformations of polymers on SLBs can be manipulated in situ. Stimuli-responsive

polymers had been used to control the protein-ligand recognition. Protein engineered to posses a reactive site near the binding site have been used to conjugated a stimuli-responsive polymer adjacent to the binding site; by changing the conformation of the polymers with temperatures, the binding events of the proteins to the ligands can be modulated.[12-14] The same concept is utilized here with the use of ELPs and will be discussed in the dissertation.

The first chapter of this dissertation emphasizes on the purpose and the objectives, background information is also included in this chapter. The experimental procedures and the analytical techniques employed in this study are described in Chapter II. Chapter III focuses on the development of a microfluidic device and the applications of the device in measuring the kinetics of PNIPAM collapse in the presence of difference salts. In Chapter IV, a systematic study of the ELPs collapse with identical sequence but different chain length is investigated. Chapter V shows the application of the ELPs on the solid supported lipid bilayers (SLBs). The ELPs conjugated SLBs show the ability to modulate ligand-receptor binding by controlling the conformation of ELPs on the surface. Finally, Chapter VI contains the conclusion of this study and the future direction of this field.

1.2 Inverse Temperature Transition

Poly(*N*-isopropylacrylamide) (PNIPAM) is a temperature-responsive polymer that it becomes insoluble and its aqueous solution becomes cloudy when the temperature is raised above the lower critical solution temperatures (LCST) as shown in Figure 1.1.

This phase transition behavior is similar to the protein folding from the cold denatuation state. The hydrophobic groups are exposed to surrounding water molecules and the conformation is in a loose extended random coil state at low temperature and transform to a compact structure above certain temperatures. The order increases both intermolecularly and intramolecularly on raising temperature in both cases therefore it is also called the inverse temperature transition. The coil-to-globule transition has been studied over decades[10,15-18] but the mechanism of the phase transition process is still not well understood.[6]

Elastin-like polypeptides (ELPs) are biopolymers consist of a repetitive pentapeptide building block, Val-Pro-Gly-Xaa-Gly. The guest residue in fourth position, Xaa, can be any amino acid but not Pro. The structure of the ELPs is shown in Figure 1.2. The ELPs undergo an inverse temperature transition[19-26] similar to the PNIPAM that the ELPs are in disordered random coils state when the solution temperature is below the LCST of ELPs. When the solution temperature is raised above the LCST, ELPs undergo a hydrophobic collapse process and assemble into a phase separated state; the former step resembles the protein folding from the cold denaturation state. The kinetics of the later step, the formation of an aqueous two-phase system[27-30], had been studied by our group[31] using a temperature gradient apparatus while the former step, kinetics of hydrophobic folding has never been studied. When the ELPs collapse, unlike the PNIPAM which collapse randomly without any structure, it is accompanied by the formation of secondary/tertiary structures similar to the protein in native state.[20,32-37] It is believed that type II β-turn structure forms when the ELPs collapse as shown in Figure

1.3, hydrogen bonds are formed between first and fourth residues in the pentapeptide repeats.[20,37-38] β-spiral, β-aggregate and distorted β-sheet might also exist.[39-43]

The thermodynamics of the PNIPAM and the ELPs collapse in the presence of Hofmeister series of salts have been studied by our group[21,44] by using a temperature gradient device.[45-47] Thermodynamics study involving in the LCST change under different conditions have been shown while the kinetic information still not clear. Experimental methods such as the dynamic laser light scattering[48-49] and the fluorescence[50-51] were used to study properties of the polymer in solution but only few of them are able to measure the kinetics of polymer collapse. Temperature jump method was applied to study the kinetics of polymer collapse trigger by temperature change but heat transfer efficiency was always a problem need to be overcome.[7,48]

Hydrophobic interactions are thought to be one of the dominant factors in the protein folding process.[52] The complex nature of the protein prevents the hydrophobic interactions to be extracted from the rest of other contributions like the polar group interactions and the protein backbone contributions. A simple model is needed to eliminate polar groups and able to extract backbone contributions from the rest in order to systematically study the role of hydrophobic interactions in the protein folding. Furthermore, the understanding of hydrophobic interaction contributions in the cold denaturation of protein is much vaguer compared to its understanding in the heat denatureation due to experiment difficulties. The cold denaturation temperature is typically estimated 20 K or more below freezing point of water[53] therefore denaturants[54]

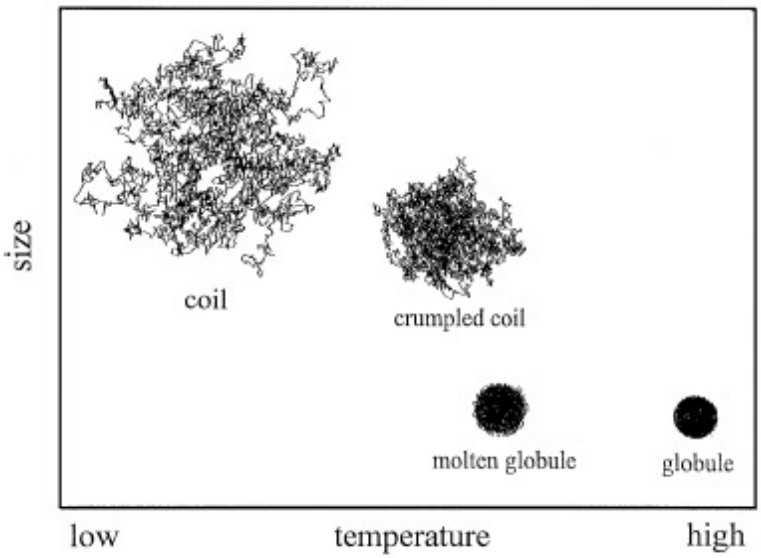

Figure 1.1. The inverse temperature transition of PNIPAM.[55]

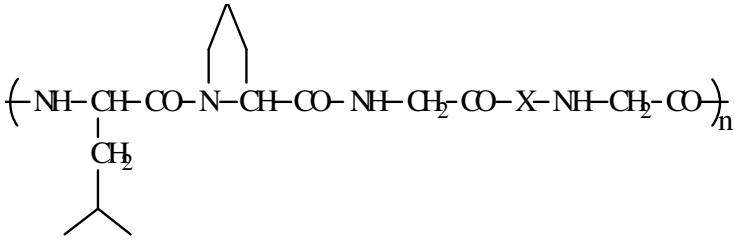

Figure 1.2. The structure of the ELP.

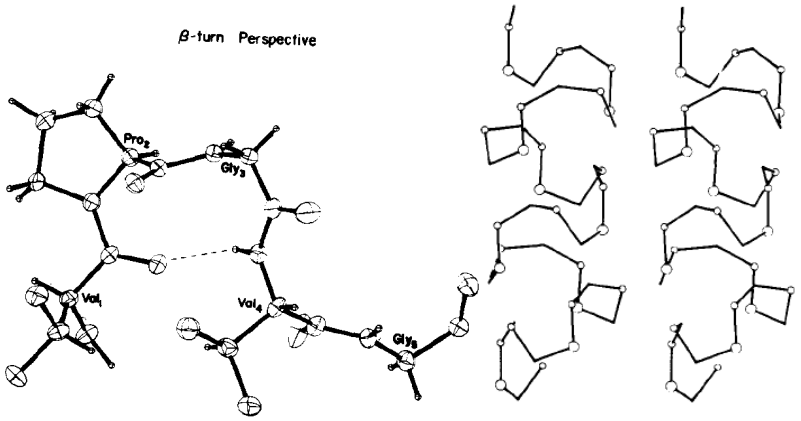

Figure 1.3. The β-turn and β-spiral of ELPs in a collapse conformation.[19]

and pH condition[56] is required to study the cold denatureation of protein and the system being studied is already disturbed.

The PNIPAM and the ELPs are good candidates to study cold denaturation of proteins and the hydrophobic interactions during the process because both of them show the inverse temperature transitions. The chain length of PNIPAM can be control precisely and the sequence and chain length of ELPs can also be precisely controlled by recombinant synthesis.[57-58] Hydrophobic backbones and hydrophobic isopropyl groups of PNIPAM provide a simple model to reveal the role of hydrophobic interactions in the collapse process. For ELPs, amino acids with polar side chains can be avoided to eliminate polar component interactions during the phase transition and the chain length could be control precisely to extract the length related backbone contributions. A set of ELPs with same compositions, wild type $V_5A_2G_3$ which means 50 percent of the guest residues are valine, 20 percent of the guest residues are alanine and 30 percent of the guest residues are glycine were used. The chain length is the variable among the four ELPs. I-30, I-60, I-120 and I-330 were used which means there are 30, 60 120 and 330 of the penta amino acid repeats in each ELPs individually, and that give 150, 300, 600, 1650 amino acids in total.

1.3 The Cell Membrane

The cell membrane which physically separates the cytoplasm from intracellular components plays an essential role in cellular process. It is composed of lipids and proteins and some carbohydrates such as glycoproteins and glycolipids. The membrane

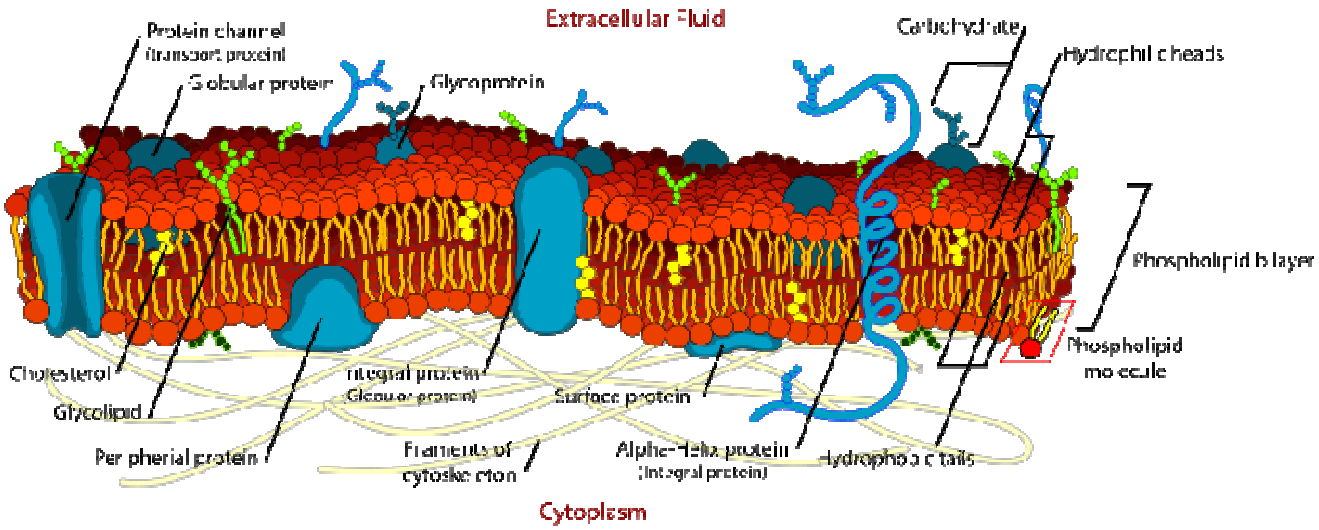

Figure 1.4. A schematic picture of cell membrane composed of a lipid bilayer and membrane proteins.[59]

provides physical support for cell and controls the permeability of substance; at the same time, many recognition events for cell signaling occur on the cell membranes.[60-61] The flows of nutrients and waste across membrane are mediated by the membrane proteins, membrane proteins also participate in communication of the extracellular environment to the intramolecular components.

Back in 1972, Singer and Nicolson presented a theory about the membrane structure known as the fluid mosaic model.[62] In the model, the cell membrane was described as a two-dimensional liquid in which lipids and proteins diffuse easily. Proteins are floating as icebergs in a two-dimensional lipid sea as described in the theory. Figure 1.4. shows a diagram representing the general structure of the cell membrane.

The main composition in the cell membranes is phospholipid, an amphipathic molecule containing a hydrophilic head and hydrophobic tails. Phospholipids include phosphatidylcholine (PC), phosphatidylethanolamine (PE), phosphatidylserine (PS), phosphatidylinositol (PI), and phosphatidylglyercol (PG). The structure of phospholipid is based on glycerol, two fatty acid chains attach to the first and second carbons of glycerol via esterification. The third hydroxyl group of glycerol reacts with phosphoric acid to form phosphatidate, further reactions of the phosphate group in phosphatidate gives other phospholipids in nature. Lipids self assemble into a bilayer structure with hydrophilic heads face toward aqueous environment and hydrophobic tails face inward and being protected from surrounding aqueous environment.[60]

The membrane fluidity is dependent on temperatures, compositions of the fatty acid and the cholesterol content. The membrane fluidity is mainly determined by the

length and the degree of unsaturation of fatty acid chains. The melting temperature of fatty acid residues in lipid has a significant effect on the membrane fluidity. The double bonds in unsaturated fatty are usually in the cis configuration and it reduces the effective packing of hydrocarbon chains. Therefore, the melting temperature decreases as degree of unsaturation increases. On the other hand, the saturated fatty acids are flexible and the melting temperature depends on the molecular weight of fatty acids.

In the cell signaling, a process called signal transduction is a mechanism transfer stimulus into cell response[60]. Series of receptors and proteins that can transduce the signal into the cell interior are involved in the process. Transmembrane receptors which have half portion sit outside the cell and other half sit inside the cell change their shape after the signal (ligand) bind to the outer part of the receptors in order to induce the signal into the cell. Although some chemical signals can pass through the cell membrane and bind to the receptors inside the cell directly, most signal transductions involve binding events outside the cell membranes[63-64] and trigger the cell response inside the cell. As shown in Figure 1.5, most signal transductions involve binding events outside the cell membranes.

1.4 Solid Supported Phospholipid Bilayers

Back in the mid 1980s, McConnell and his coworkers introduced supported lipid bilaysers[65-67] (SLBs) to mimic cell membranes (Figure 1.6).[68] It possesses the lateral lipid mobility similar to the cell membranes. The lateral lipid mobility is the fundamental property of cell membranes[69-70] and it makes solid the SLBs as an ideal

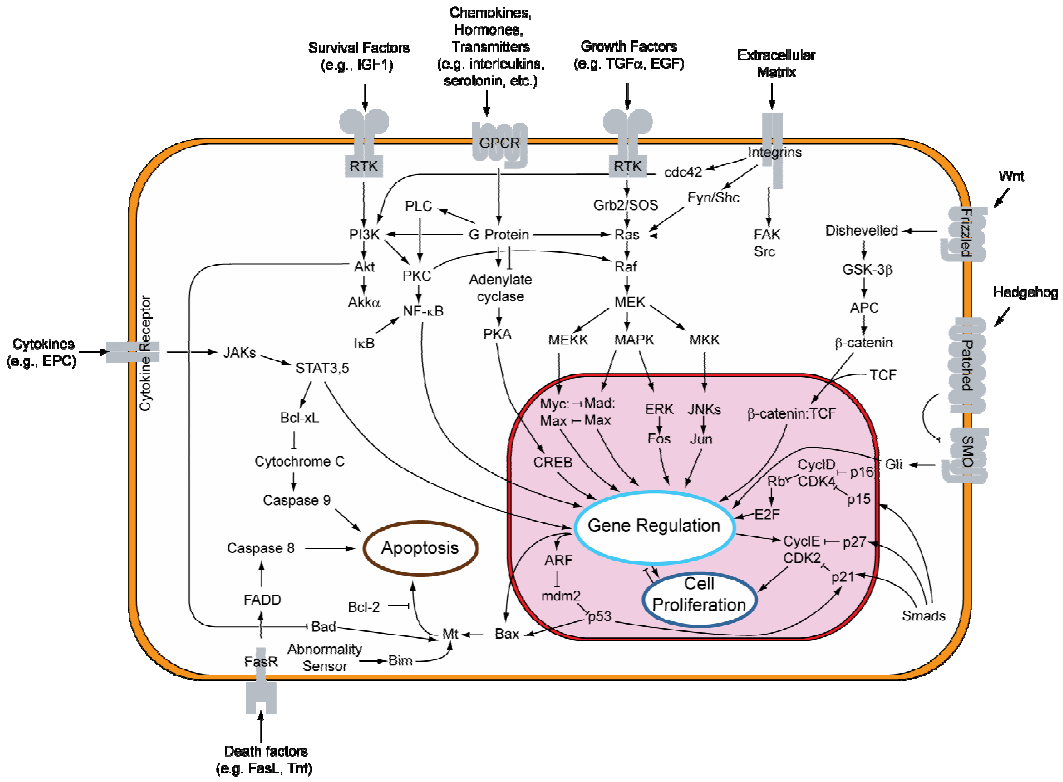

Figure 1.5. Overview of signal transduction pathways. The image was adapted from www.wikipedia.org.

platform for biosensing because this two-dimensional rearrangement is similar to cell membrane surface ligand-receptor recognition events.[71-74] The SLBs are widely used to study the biological membranes properties[75] such as ligand-receptor binding[76-77] and interactions between lipid and protein.[78-80] It is also utilized in sensing,[81] drug discovery[82] and separation[83-86] applications. A thin layer of water molecules is trapped between the bilayer and the solid support[87-90]; this water layer maintains the lateral mobility of bilayers and allows the reorganization of membrane components.

SLBs can be made by two general methods. In the first method, the lower leaflet of the bilayer is formed by Langmuir-Blodgett technique. The hydrophobic tails of lipids from air-water interface orient themselves toward the air and the polar head groups will face water. When a hydrophilic substrate is pulled out from water surface, a monolayer will form on the substrate. The upper leaflet is formed by horizontally dipping the substrate through another lipid monolayer by a Langmuir-Schaffer procedure (Figure 1.7).[66] The second method which is employed in this study is a vesicle fusion method(Figure 1.8).[65,67] SLBs are formed through spontaneous adsorptions and fusions of small unilamellar vesicles (SUVs) to a planar solid substrate. The SUVs were prepared through vesicle extrusions[91-93] in this study while sonication method[94] is also used to prepare SUVs. Briefly, the lipids with desired compositions were mixed from stock solutions in chloroform. The solvent were then removed by a stream of nitrogen and further dried under vacuum. The lipids were then rehydrated by adding buffer and subjected to 10 freeze-thaw cycles in order to transform multilamellar vesicles into large unilamellar vesicles. 8 times of extruding through two stacked polycarbonate membranes

with 100 nm pores make vesicles with uniform size. The SUVs prepared by this procedure were 100 ± 10 nm in diameter as determined by the dynamic light scattering.

The SUVs with size between 50-100 nm have high radius of curvature[95] and therefore can be used in vesicle fusion method to prepare SLBs. When vesicle solutions are exposed to smooth and clean[68,75] hydrophilic planar surface like borosilicate glass, mica, oxidized Si, fused quartz[66,96-97], SUVs spontaneously fuse to the surface to form single lipid bilayers.[71,98-99] The process involves absorption of the vesicles to the surface, followed by rupturing and fusing to form a continuous lipid bilayers, however, the actual mechanism is still not well understood.

1.5 Summary

Despite the importance of the protein folding in biochemistry, the understanding of its mechanisms and the roles played by each component such as hydrophobic interactions are still not well understood, moreover, the protein cold denaturation is still vague in mechanisms and is hard to access for most of proteins. The first goal of this study is to employ simple models like PNIPAM and ELPs to study to the kinetics of hydrophobic interactions and the role of hydrophobic interactions played in a process resembles protein cold denaturation.

A new microfluidic system is built with a temperature jump in order to trigger the PNIPAM and ELPs collapse process. The small dimensions of the microfluidics allow smaller sample consumption and overcome the heat transfer efficiency problem as seen in previous research. The effects of different temperature change, different salts and

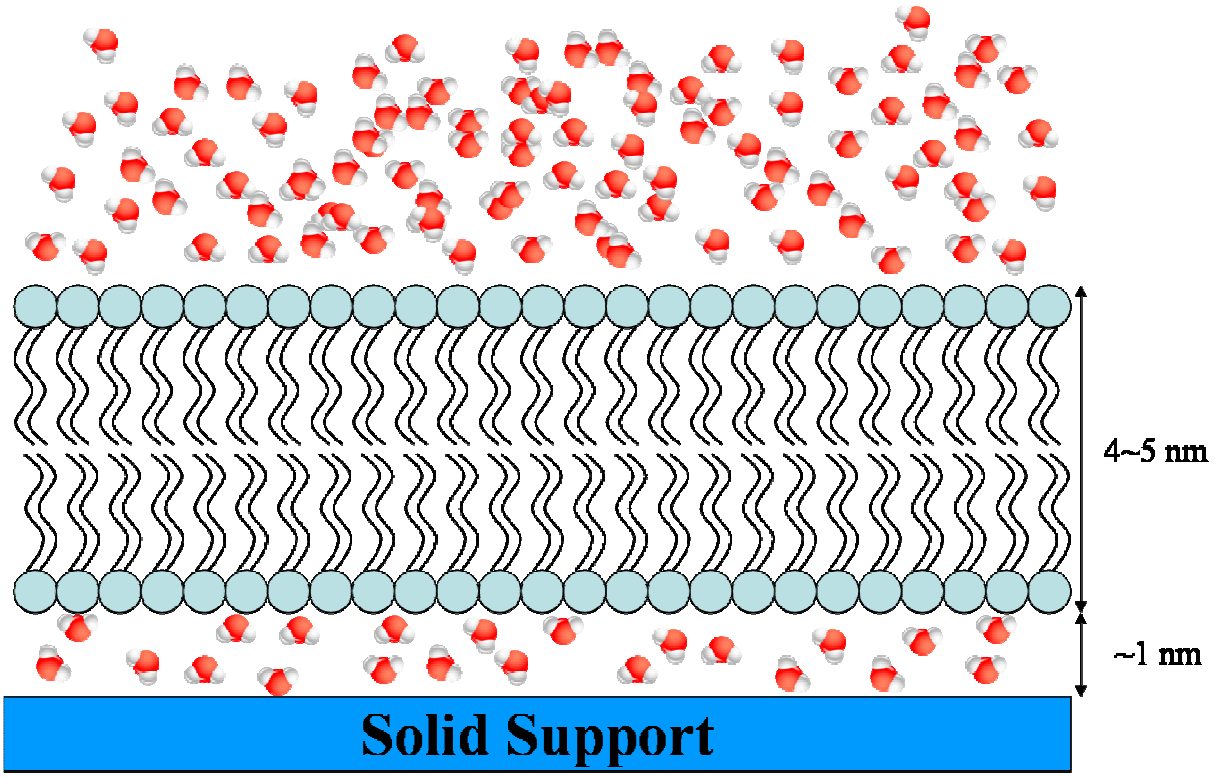

Figure 1.6. Schematic diagram of supported lipid bilayers on a hydrophilic substrate. A thin layer of water molecules about 1 nm thick is trapped between the bilayer and the solid support

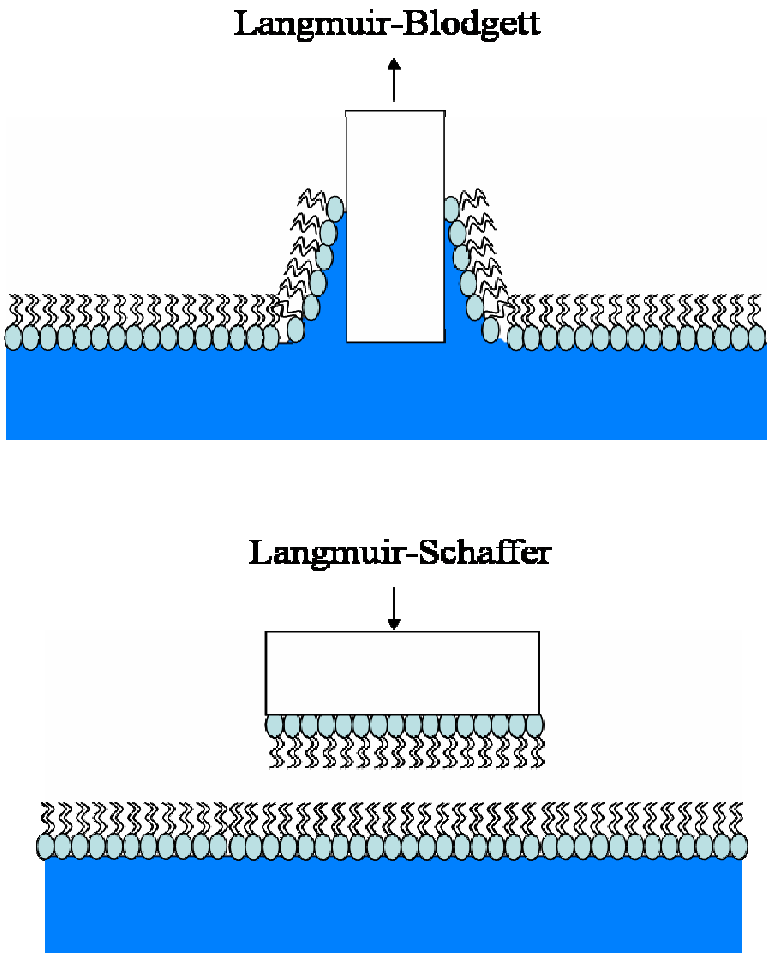

Figure1.7. Langmuir-Blodgett pulling for lower leaflet and Langmuir-Schaffer for upper layer.

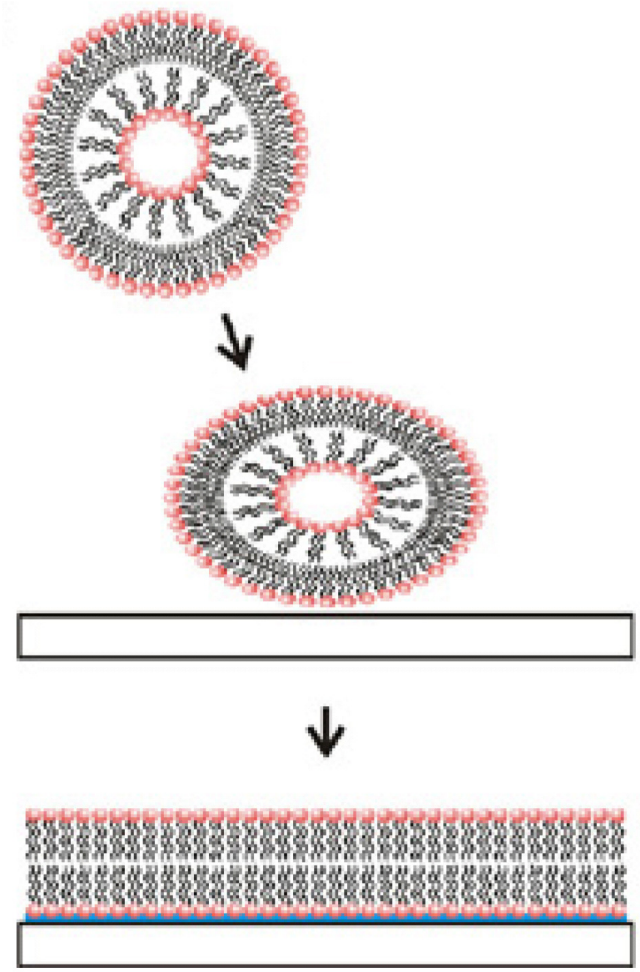

Figure 1.8. Spontaneous formation of solid supported lipid bilayer by vesicle fusion method.[75]

different polymer length will be studied and the data obtained by kinetic measurement can used to calculate thermodynamic parameters allowing us to have better understanding to the process of polymer hydrophobic collapse.

In the other part, solid supported phospholipid bilayers are utilized to mimic the cell membrane and the ELPs conjugated on the surface are utilized as a tunable filter to either allow or block protein binding to the ligand on the membrane surface. The second goal of this study is to improve the technology of supported lipid bilayers and broaden its applications. The conformation of ELPs conjugated on membrane surface can be modulated in an extended coil conformation or a compact globule conformation by changing temperatures or changing buffer compositions. The advantage of this design is the conformation of the polymers on the surface can be controlled in situ compared to previous design where the conformation was predetermined by the density of the polymer on the surface.

Overall, the study of the PNIPAM and ELPs collapse by a novel temperature jump microfluidics and the applications of ELPs on solid supported lipid bilayers will be shown in this dissertation.

CHAPTER II

EXPERIMENTAL

2.1. Synopsis

This chapter presents the experimental information employed through this study. Starting from the introduction of fabricating temperature jump microfluidics; a novel device is developed in this study. Then the preparation of elastin-like polypeptides used in collapse kinetic study is introduced through of *E. coli.* expression. In the later section, the fabrication of microfluidic device employed in SLBs study via soft lithography is discussed followed by the method of labeling protein with the fluorescent dye. Applications of microfluidic technology[100] combined with SLBs as analytical platform is discussed in this chapter. Some techniques such as fluorescence recovery after photobleaching (FRAP)[101] which is used to determine two-dimensional lateral fluidity is only employed to check the quality of SBLs and it will not be discussed in this chapter.

2.2. Temperature Jump Microfluidics

A novel T-jump device was utilized to measure the kinetics of the PNIPAM and ELPs collapse triggered by different temperatures. This device was adapted from the temperature gradient device[44-47,100] developed in our group. Instead of using a hot source and a cold sink, two parallel brass tubes were both used as hot source and the channel was parallel to the brass tube instead of perpendicular placement in order to provide a larger detection window. A cover glass acting as both sample stage and heat conductor

was mounted on top of the two parallel brass tubes. The stainless steel sheath heaters were placed inside the brass tubes and connected to the variable autotransformer. The square capillary tube (0.1 × 0.1 mm) was fixed on the cover glass and connected to a plastic tube by capillary wax. The plastic tube was connected to a peristaltic pump tube mounted on a peristaltic pump and the flow of sample was controlled by this peristaltic pump. Light scattering from polymer solutions was monitored via a CCD camera using dark field optics under an inverted microscope. The device figure is shown in Figure 2.1.

The collapse process of the PNIPAM and ELPs were triggered by a temperature jump as PNIPAM/ELPs solution entered heated capillary tube in the middle of heating brass tubes from room temperature plastic tube. The collapse process proceeded along the capillary tube as PNIPAM/ELPs solution traveled in the tube. Series of pictures were taken along the capillary tube in order to catch the interface of light scattering. The light scattered increased significantly after PNIPAM and ELPs collapsed closed to globule conformation and could be observed by the dark field microscopy. Position of light scatter intensity started to increase was set as end point where the collapse process was approaching to the end. Time needed for PNIPAM/ELPs to collapse could be obtained by calculating the time needed for solution to travel from temperature jump position to the light scattered interface position since the dimensions of the capillary and the flow rate are known. This is the first time a device shows the ability to measure PNIPAM and ELPs collapse by trigger by a temperature jump in a continuous flow form. The device could be considered as a combination of the temperature jump method and the

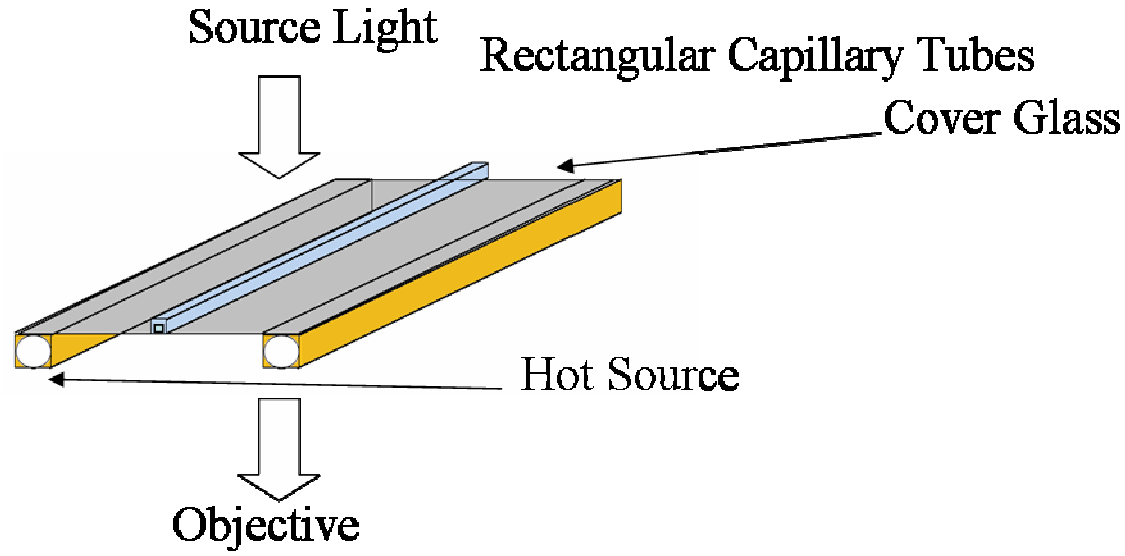

Figure 2.1. The temperature jump microfluidics.

continuous flow method. In the latter chapter, more detail will be discussed such as the heat transfer and the temperature along the capillary.

2.3. Preparation of Elastin-Like Polypeptides

The pET plasmids employed in this study were constructed by recursive directional ligation (RDL) as previously described[57] by Dr. Chilkoti's research group in Duke University to synthesis the repetitive polypeptides of a specified chain length. The plasmids were then expressed in BLR/DE3 *E. coli* in TBdry which is high growth media, with ampicillin as a selective agent for 24 h in the shaker at 37 °C, 300 rpm. The purification of the ELPs was started from sonication of the cells to lyse the cell and release ELPs. The total sonication time was 10 minutes with 10 seconds on and 20 seconds off intervals to prevent overheating the solution. This process was done in a cold room and the solution was kept in a bucket of ice. Then the cell lysate was removed by centrifuging at 4 °C, ELPs stayed dissolved at low temperature so the supernatant was kept for further purification.

Polyethylamine was added into the supernatant as 0.5 % w/v final concentration. Another low temperature centrifuge was conducted to remove insoluble DNA and RNA. This step was followed by a series of inverse transition cycling (ITC) steps. One round of ITC was carried out by centrifugation at 10000g under 50 °C by adding 2 M NaCl (the temperature and NaCl concentration varies with ELPs, for an ELPs with higher LCST, higher temperature and more concentrated NaCl is required). The high temperature and salt were employed to cause ELPs collapse so that ELPs can be

collected in the pellet after centrifuge. The pellet (which contains ELPs) was then dissolved in cold PBS buffer, and the remaining cellular debris was removed by centrifugation at 10000g. Typically, one or two rounds of ITC were needed to remove impurities.

The concentrations of the purified ELPs solutions were determined by measuring the absorbance at 280 nm ($\varepsilon = 5690\ M^{-1}\ cm^{-1}$). After purified by ITC, samples were dialyzed against purified water for several days to remove residual salts. Finally, the samples were lyophilized by vacuumed liquid nitrogen frozen samples to remove water and stored at -80 °C until use.

2.4. Preparation of Microfluidic Device by Soft Lithography

Soft lithography developed by Whitesides and coworkers[102-104] refers to a set of methods for fabricating structures using elastomeric materials, polymeric stamps and conformable molds. It is convenient, low cost and effective method compare to other lithography methods such as photolithography and electron beam lithography to create a micro- or nanostructures[46,96,99,105-106] and it is widely used in biotechnology and plastic electronics.

The first step of soft lithography, photolithography step, is to transfer desired pattern or structure from a photomask to a glass slide coated with photoresist polymer by UV radiation. The next step is developing the exposed glass slide by chemical etching or dry etching[103] to create a photomaster. The final step is to transfer the negative image on

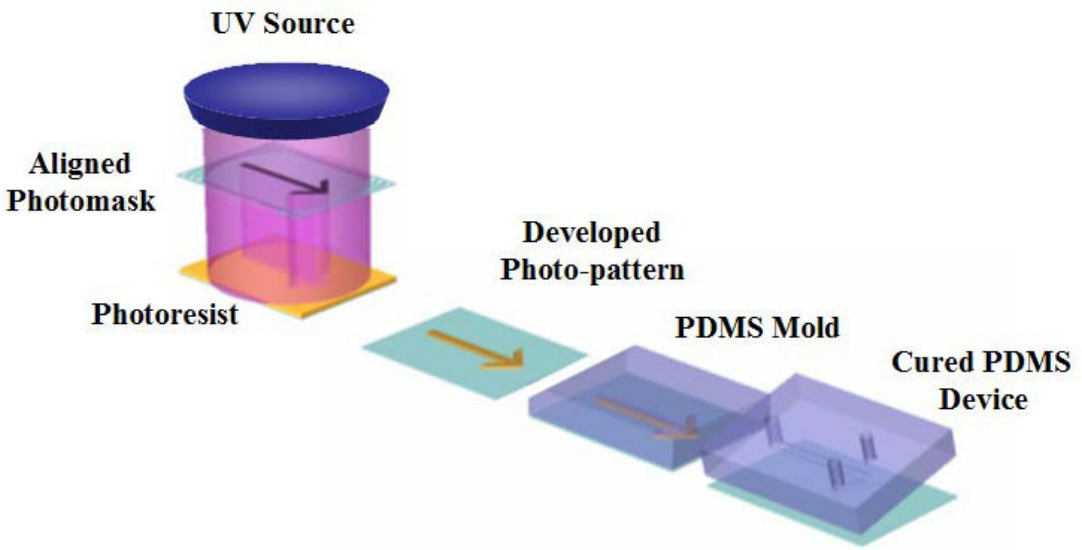

Figure 2.2. Schematic diagram represents the process of soft lithography to prepare microfluidic device.[107]

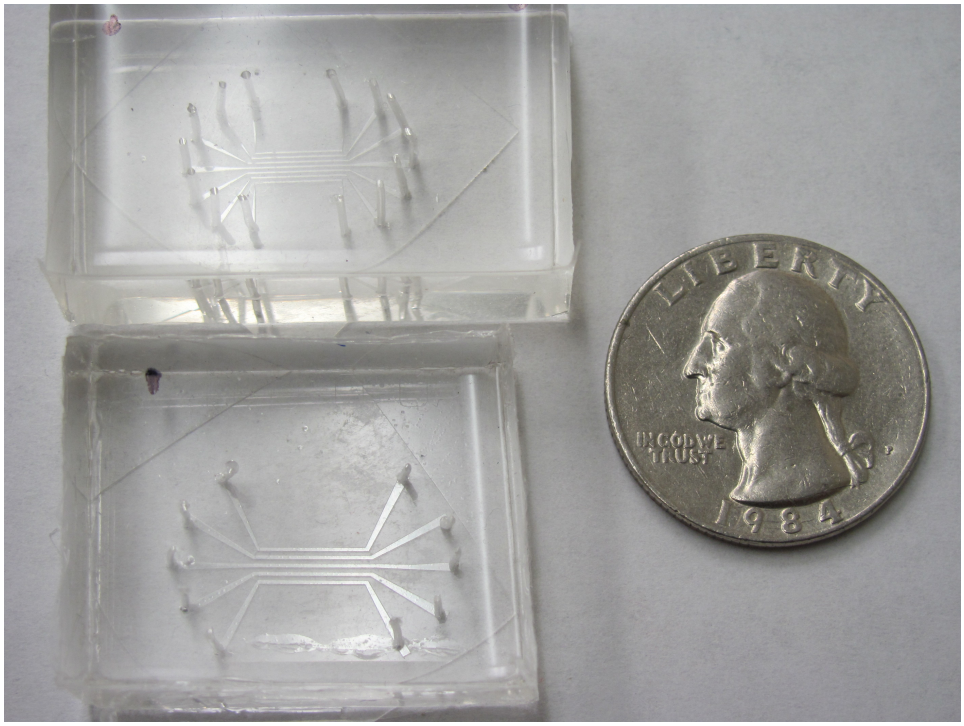

Figure 2.3. The 5 and 7 channels PDMS microfluidic devices used in this study.

the photomaster to a poly(dimethylsiloxane) (PDMS) chip by pouring the degassed precursor of PDMS on top of the photomaster.

Briefly, the glass substrate is spin coated with a layer of photoresist and exposed to UV light through a photomask with desired image. This glass is then treated with developing solution and baked at 120 ^{o}C overnight. Buffered oxide etchant (BOE), 1:6 ratio (v/v) of 48 % HF and aqueous NH_4F (200 g in 300 mL purified water) are used to etch the glass. The quality of the pattern on the glass slide is checked with a profilometer. After the photoresist are removed by acetone, the patterned glass substrates were ready to be used as molds to make microfluidic device. Next, the a mixture of PDMS precursor is degassed under vacuum and poured over the photomaster and cured at 55 ^{o}C for overnight. A glass slide cleaned in a boiling solution of ICN 7X and purified water ratio is placed in oxygen plasma with cured PDMS for 10 s, them these two pieces are brought into contact to create the microfluidic device. The glass slide was annealed in a kiln at 500 ^{o}C for 5 h before introducing to oxygen plasma.

2.5.Conjugation of Fluorescently Labeled Protein

In order to detect the binding event of protein to the ligand on the membrane surface, the protein must be labeled with fluorescent dye. This procedure is carried out by using Alexa Fluor-594 with succinimidyl ester reactive moiety. Alexa Fluor dyes are brighter, less pH sensitive than Texas Red with equivalent excitation and emission wavelengths. Furthermore, Alexa Fluor dyes possess higher quantum efficiency, chemical and thermal stability and high solubility in aqueous solutions. The ELPs filter

is design to be modulated by ionic strength and temperature therefore, the pH sensitivity must be low and the thermal stability must be high for the employed dye.

Figure 2.4 shows the chemical structure of Alexa Fluor 594 and the label reaction. The label process is performed in the presence of sodium bicarbonate to give a desire pH environment (> pH 7). The succinimidyl ester on the dye molecule reacts with the primary amine on the protein to form a stable dye-protein conjugates, this reaction is carried out at low temperature overnight. Size exclusion chromatography is used to separate the unreacted dye and the labeled proteins.

2.6.Conjugation of ELPs with SUVs

The primary amine of ELPs is used as a reactive group to couple with the carboxylic acid on the lipid for the filter purpose in Chapter V. The ELPs used for this study is ELP$[V_2I_7E]_{120}$. The carboxylic acid is provided by 1,2-dipalmitoyl-sn-glycero-3-phosphoethanolamine-N-(glutaryl) as shown in Figure 2.5. The reaction is conducted with the use of 1-Ethyl-3-[3-dimethylaminopropyl] carbodiimide hydrochloride (EDC) and *N*-hydroxysuccinimide (NHS) which are provided by Pierce Biotech. The vesicles are first reacted with EDC/NHS to form a semistable amine-reactive NHS-ester and then the ELPs are introduced in the solution to react at low temperature for 24 h to form ELPs conjugated vesicles. The general reaction scheme is shown is Figure 2.6.

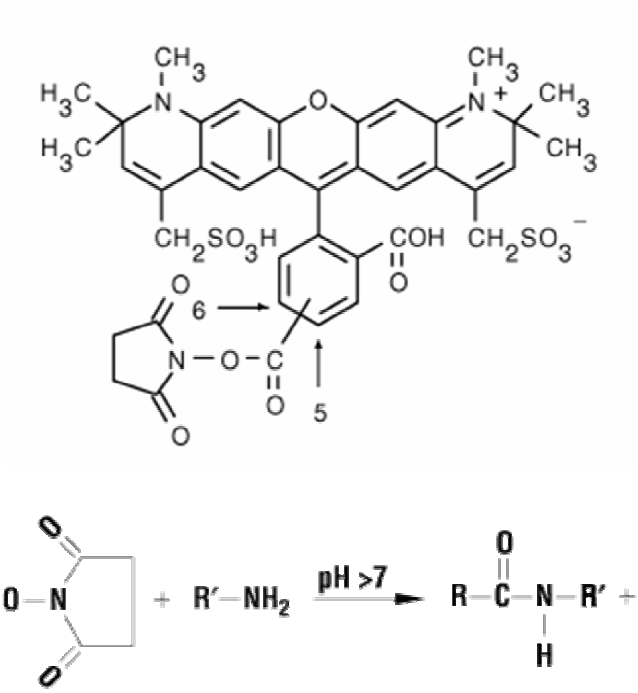

Figure 2.4. The structure of Alexa Fluor 594 carboxylic acid, succinimidal ester and the reaction between succinimidal ester and primary amine.

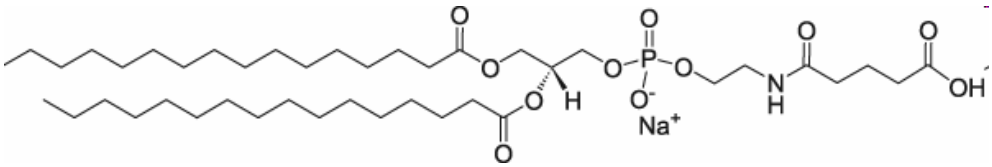

Figure 2.5. The structure of 1,2-dipalmitoyl-sn-glycero-3-phosphoethanolamine-N-(glutaryl) that provide carboxylic acid reaction group to couple with ELPs.

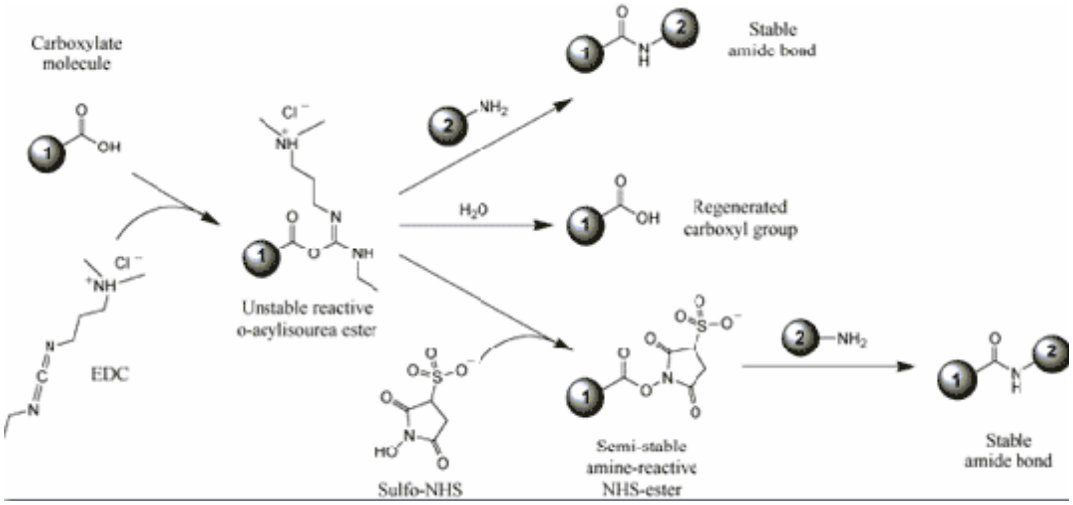

Figure 2.6. The EDC/NHS coupling reaction. (http://www.piercenet.com)

CHAPTER III

NON-ARRHENIUS BEHAVIOR OF PNIPAM COLLAPSE AND THE EFFECTS OF SALTS MEASURED BY T-JUMP CONTINUOUS FLOW DEVICE

3.1. Synopsis

We introduce a new device to study the kinetics of the coil-to-globule transition of poly(*N*-isopropylacrylamide) (PNIPAM). This new setup combines the temperature jump method and the continuous flow method and it is suitable to measure millisecond timescale process. Sufficient heat transfer was confirmed by fluorescence measurements of rhodamine b. The PNIPAM collapse triggered by temperature jumps exhibited similar behavior to protein as reflected in the slope changes at different temperatures in the Arrhenius plot. As the temperature is raised, the PNIPAM collapses faster and the rate enhancement becomes smaller at elevated temperature. According to the transition state theory, enthalpy, entropy change of activation and the change of heat capacity values at transition could be calculated by fitting the 1/T versus ln k/T (Eyring Plot). The effects of different salts in the Hofmeister series to the collapse kinetics were also studied. In the presence of 0.2 M chloride (which increases the LCST of PNIPAM by 2 degrees), it was found that as PNIPAM collapses faster, the thermodynamic parameters got smaller. On the other hand, in the presence of 0.2 M thiocyanate which raises the LCST of the PNIPAM by about 0.9 degree, the rate of the PNIPAM collapse does not change much while the thermodynamic parameters have larger values compared with the PNIPAM collapse in the absence of salts. Salts show the ability of changing the conformation of

PNIPAM and the obtained thermodynamic values agree with the previous LCST study of PNIPAM.

3.2. Introduction

A new device combining temperature jump and continuous flow method is introduced here to study the kinetics of poly(*N*-isopropylacrylamide) (PNIPAM) collapse triggered by temperature jump as a model of the protein folding study.

The protein folding is one of the fundamental problems in biophysics. It involves how protein folds from a random structure to a compact native structure in which it possess activity.[1] Knowing the pathway and the mechanism of the protein folding may provide more information in understanding the structures and the functions of thousands of protein sequences.[4] The mechanism and the dynamic of protein folding are still not clear[2-3] especially for the folding and denaturing during the cold denaturation of protein. The understanding of the cold denaturation is far less compare to heat denaturation due to the fact that cold denaturation always occurs below freezing temperature of water and is hard to be studied in aqueous solution.[5]

PNIPAM is a good candidate to be used as a simple model to study the cold denaturation of protein: study of polymer chain collapse from a random coil to a compact globule conformation provides some clues of the initial stage of the protein folding.[7] Coil-to-globule transition of polymer has been studied over decades[15-18] and the equilibrium properties of the polymer in dilute solution have been well studied.[108] On the other hand, the mechanisms of the polymer chain collapse is still not clear.[6] There are

some numeric ways to simulate polymer system by computer[109] such as Langevin equation[110] and Monte Carlo simulation[111] but numbers of success experimental method to measure coil-to-globule transition is still few.

PNIPAM is known to be insoluble above its lower critical solution temperature (LCST). It collapses above the LCST and the polymer makes solution cloudy. The collapse behavior of the PNIPAM is similar to the refolding of protein in cold denaturation. In both process, hydrophobic moieties are exposed to water molecules at lower temperature region and become compact structures above the critical temperature. Our group had studied the ion effects of the Hofmeister series on the LCST of the PNIPAM[44] by a temperature gradient device.[45] However, the collapse kinetics of this homopolymer is not fully understood although different states have been observed during coil-to-globule transition.[55,112-113] Some experimental methods such as the laser light scattering[48-49] and the fluorescence[50-51] were used to study the properties of polymers in solution but only few of them are able to measure the dynamic of polymer collapse triggered by series of different temperatures. Temperature jump method was applied to study the kinetics of polymer collapse but heat transfer was always a problem.[7,48]

The collapse kinetics of PNIPAM under different temperatures was investigated and the effects of salts on the PNIPAN collapse kinetics was also studied here by this new platform. Thermodynamic parameters of PNIPAM collapse in different conditions can be calculated via transition state theory which might provide more clues in polymer chain collapse and in protein folding.

3.3.Experimental

Sample Preparation. All the inorganic salts and rhodamine B used in these experiments were purchased from Aldrich. Low-conductivity H_2O, produced from a NANOpure Ultrapure Water System (Barnstead, Dubuque, IA) with a minimum resistivity of 18 MΩ·cm, was used to prepare the polymer and salt solutions. Stock solutions of PNIPAM at 20 mg/mL were prepared by allowing the polymer to dissolve overnight in H_2O at 4 °C. Aliquots of these solutions were added to water or inorganic salt solutions at the desired concentration. The final polymer concentration for all experiments performed herein was 10 mg/mL.

Fabrication of Temperature Jump Flow System. A cover glass (22 × 22 mm, VWR, West Chester, PA) acting as both sample stage and heat conductor was mounted on top of two parallel brass tubes. Stainless steel sheath heaters (Omega Engineering inc., Stamford, CT) were placed inside brass tubes and connected to variable autotransformer (Staco Energy Products Co., Dayton, OH) to control temperature (Figure 1a).

Square capillary tube (0.1 × 0.1 mm, Fiber Optic Center Inc., New Bedford, MA) was fixed on a cover glass and connected to a plastic tube by capillary wax (Hampton Research, Aliso Viejo, CA). The plastic tube was connected to a peristaltic pump tube mounted on a peristaltic pump (Harvard Apparatus, Holliston, MA) and the flow of sample was controlled by this peristaltic pump. Light scattering from polymer solutions was monitored via a CCD camera (Micromax 1024, Princeton Instruments) using dark field optics under an inverted microscope (Nikon, TE2000-U).

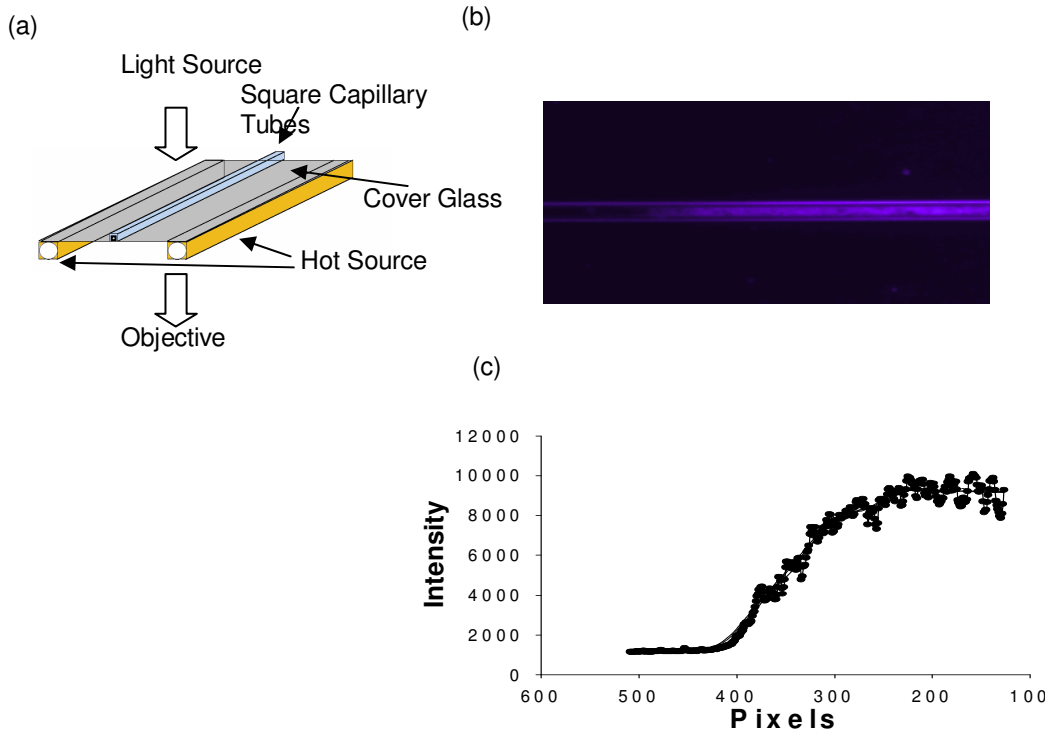

Figure 3.1. (a) The setup of T-jump continuous flow device, capillary tube was placed in the middle of two hot sources to ensure temperature uniformity along capillary tube. (b) light scattering of PNIPAM and interface. (c) line scan of PNIPAM solution near interface shows dramatic increase of light scattering intensity.

3.4.Results and Discussion

Kinetics PNIPAM Collapse. Figure 3.1 shows the setup of the device and typical data obtained from the device. The collapse process was triggered by a temperature jump as the PNIPAM solution (MW300000, 10 mg/mL) entered the heated capillary tube in the middle of two heated brass tubes from room temperature plastic tube.

High temperature was set to insure full collapse of PNIPAM (322.7 K). Collapse process proceeded along capillary tube as the PNIPAM solution flowed in the tube. Series of pictures were taken along the capillary tube to catch the interface of the light scattering. The light scattering increased significantly after the PNIPAM collapse process approached to end and could be observed by a dark field microscopy as shown in Figure 3.1b. Position of light scatter intensity started to increase was set as the end point where the collapse process approached to end. Time required for PNIPAM to collapse could be obtained by calculating the time spent for PNIPAM to flow from temperature jump position to the light scattered interface since the dimensions of the capillary and the flow rate are known. Concentration being used here is relatively high (10 mg/mL) therefore the collapse process involves multiple PNIPAM chain aggregations. The collapse rate obtained under this condition is 94.8±3.3 ms. This time scale is close to previous study of the single PNIPAM collapse triggered by mixing solvent.[114] To the best of our knowledge, this is the first measurement of PNIPAM collapse by temperature jump in a continues flow device.

Heat transfer was always a problem in the study of polymer collapse triggered by temperature jump.[7,48] Microfluidic system used here reduced the sample volume therefore the heat required to achieve temperature jump was also reduced. Rate of heat transfer was confirmed by fluorescence measurement of rhodamine B along the length of capillary tube. The fluorescence of rhodamine B is temperature dependent and can be used as a temperature indicator.[115-116] After subtracting background fluorescent (fluorescence of static rhodamine B at room temperature), the fluorescence of rhodamine B shows intensity drop in interface of temperature jump and becomes flat after the drop along the capillary under the same condition used as in the PNIPAM measurement (Figure 3.2., Figure 3.3.). This result implied that the temperature jump takes 10 ms and the temperature is uniform along the capillary under the flow rate and the temperature set and therefore, the heat transfer rate is sufficient for PNIPAM collapse measurement.

Kinetics Analysis. There is not much literature can be found dealing with the kinetics of polymer collapse involving multiple chain aggregation and we found that the kinetic parameters could be fit nicely with the transition state theory. As mentioned, the collapse rates of PNIPAM measured in this study are closed to the rate of the single PNIPAM collapsed in previous study,[114] which indicates that the rates measured here are the formations of the PNIPAM particles formed due to PNIPAM collapse involving multiple chain aggregation, not the growth of PNIPAM particles after collapse due to particle aggregations. By fitting kinetic parameters with the Eyring plot which is derived from the Arrhenious equation, we are able to get thermodynamic parameters involved in

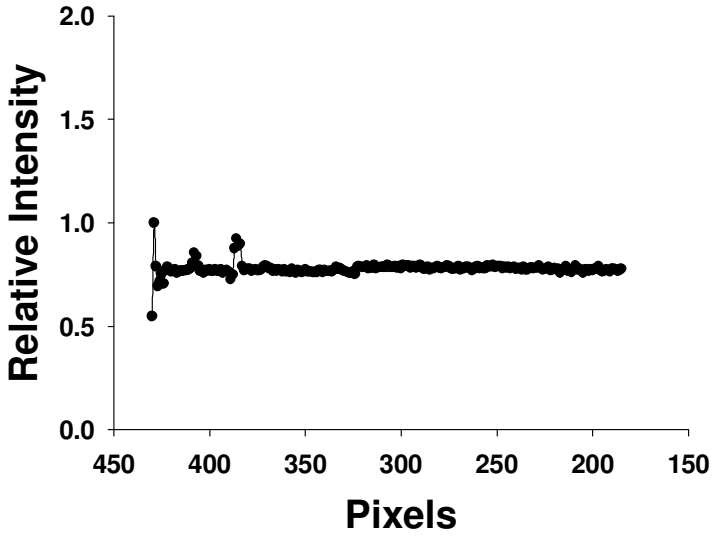

Figure 3.2. Fluorescence intensity of rhodamine B (2.5 mM) measured in T-jump continuous flow device under the same condition as the PNIPAM collapsemeasurement. The relatively flat intensity along the capillary tube shows uniformity of temperature.

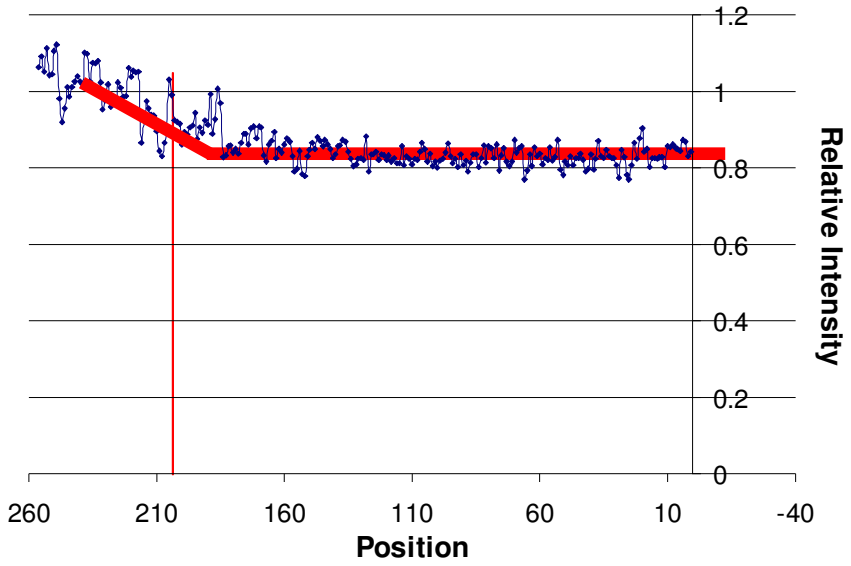

Figure 3.3. 10 ms temperature jump of the device as shown in rhodamine B measurement.

collapse process. This method is similar to the protein denature study.[117-118]

The activation free energy ($\Delta G^{0\ddagger}$) of PNIPAM collapse can be calculated by transition state theory as shown in equation 1.[10]

$$k = \frac{\kappa k_b T}{h} \exp\left[-\left(\frac{\Delta G^{0\ddagger}}{RT}\right)\right] \qquad (1)$$

where k_b is Boltzmann constant, h is Plank's constant, R is the gas constant. κ is the transmission factor with an upper limit of 1. This transmission factor is smaller in solution and will lead to the observed activation free energy to be smaller than absolute value.

Free energy can be written as $G = H - TS$. Activation enthalpy and activation entropy are temperature dependent as shown in eq 2 and eq 3.

$$\Delta H^{\ddagger}(T) = \Delta H^{\ddagger}(T_0) + \Delta C_p^{\ddagger}(T - T_0) \qquad (2)$$

$$\Delta S^{\ddagger}(T) = \Delta S^{\ddagger}(T_0) + \Delta C_p^{\ddagger} \ln(T / T_0) \qquad (3)$$

$\Delta C_p^{\ddagger}$ is the change of heat capacity at constant pressure in transition state. The change of heat capacity is assumed to be temperature independent in the temperature range studied.

From eq 2 and eq 3, free energy of activation can be written as

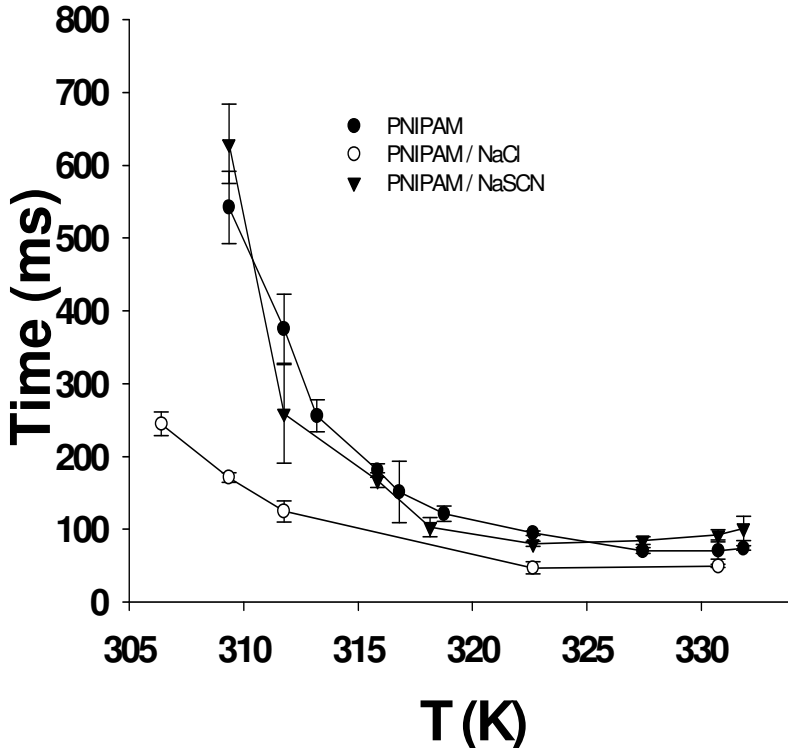

Figure 3.4. Temperature vs collapse rate of 10 mg/mL PNIPAM solution, 10 mg/mL PNIPAM with 0.2 M NaCl solution, and 10 mg/mL PNIPAM with 0.2 M NaSCN solution.

$$\Delta G^{\ddagger}(T) = \Delta H^{\ddagger}(T_0) - T\Delta S^{\ddagger}(T_0) + \Delta C_p^{\ddagger}[(T - T_0) - T\ln(T/T_0)] \quad (4)$$

After substitution of eq 4 into eq 1 and rearrangement we can get an expression of temperature dependent rate constant

$$\ln\frac{k}{T} = \ln\frac{\kappa k_B}{h} + \frac{\Delta S^{\ddagger}(T_0)}{R} - \frac{\Delta C_p^{\ddagger}}{R} - \frac{\Delta C_p^{\ddagger}}{R}\ln T_0 + \left(\frac{\Delta C_p^{\ddagger}(T_0)}{R} - \frac{\Delta H^{\ddagger}(T_0)}{R}\right)\frac{1}{T} + \left(-\frac{\Delta C_p^{\ddagger}}{R}\right)\ln\frac{1}{T} \quad (5)$$

Consequently, by plotting the ln(k/T) against 1/T(Eyring plot) and fitting the plot with Y=A+BX+ClnX, $\Delta C_p^{\ddagger}$, $\Delta S^{0\ddagger}$, and $\Delta H^{0\ddagger}$ values under standard state (298.15 K) [119] can be calculated respectively. Enthalpy and entropy change of activation at different temperature can also be calculated by eq 2 and eq 3. Due to the uncertainty of transmission factor, the obtained values of $\Delta S^{0\ddagger}$ represent apparent entropy of activation while the value of $\Delta H^{0\ddagger}$ represent the actual enthalpy of activation.

The kinetics of PNIPAM collapse triggered by different temperatures is shown in Figure 3.4. The rate of collapse increased as temperature increased in lower temperature region and the rate increment became smaller at elevated temperature away from LCST of PNIPAM. The collapse kinetics flattened around 330 K. Figure 3.5. shows the Arrhenius plot of the PNIPAM collapse; instead of a commonly observed linear regression in the Arrhenius plot as of simple chemical reactions, non-Arrhenius behavior is shown for the first time as PNIPAM collapse and this behavior is similar to protein folding.[117,120-121] The curve showed linear trend at lower temperature part and

derived from linear at higher temperature which indicates the collapse was dominated by enthalpy at lower temperature and entropy takes over at high temperature.[122-123]

Plotting 1/T vs ln k/T (Eyring plot) and fitting this plot with eq 5, thermodynamic parameters such as heat capacity change at transition state, enthalpy change of activation and entropy change of activation under standard state (298.15 K) can be calculated (Figure 3.6). The values of activation obtained are listed in Table 3.1 showed same order as small peptides folding value obtained via transition state theory by different experiment methods.[117-118] These values are several times larger compare to single peptide folding due to longer length of PNIPAM (MW300000) used and the possibility of multi-chain association due to high concentration used in PNIPAM study.

Positive entropy change of activation is observed although the contribution of entropy change from PNIPAM configuration should be negative. This positive value is contributed by the water structure being more disordered at transition state as a result of the partial PNIPAM hydrophobic collapse. Water molecules around hydrophobic surface have limited orientation in order to keep hydrogen bonds with other water molecules. Partial collapse of PNIPAM in transition state reduced the hydrophobic surface exposed to water and released water from hydrophobic portion therefore increases system entropy.

More conformations are accessible for water molecules around hydrophobic portion of the PNIPAM when the temperature goes higher. Some of the conformations have weaker or unformed hydrogen bonds and weaker van der Waals interactions (therefore higher energy), this behavior contributes to heat capacity since the system energy increases with temperature.[124-125] This contribution of heat capacity reduced as

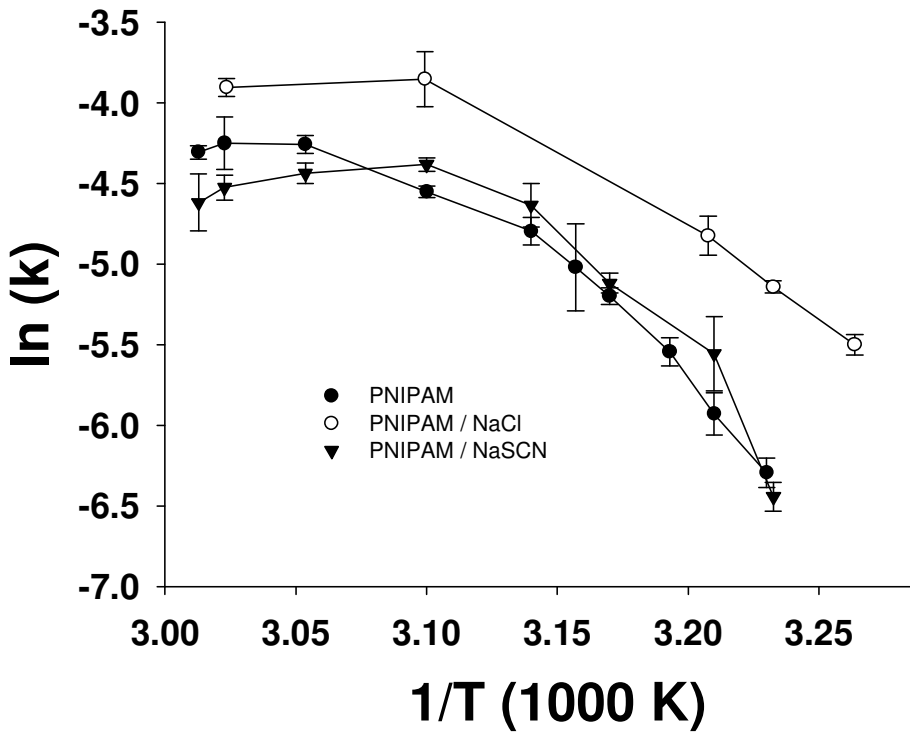

Figure 3.5. Arrhenius plot of 10 mg/mL PNIPAM solution, 10 mg/mL PNIPAM with 0.2 M NaCl solution, and 10 mg/mL PNIPAM with 0.2 M NaSCN solution with error bar.

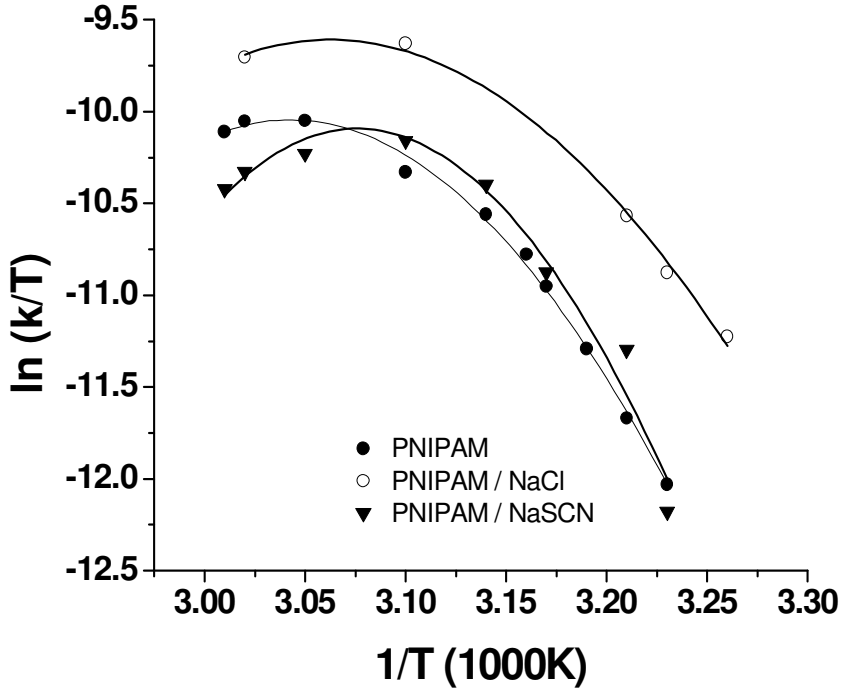

Figure 3.6. Eyring plots of 10 mg/mL PNIPAM solution, 10 mg/mL PNIPAM with 0.2 M NaCl solution, and 10 mg/mL PNIPAM with 0.2 M NaSCN solution. Fitting of this plot by y=A+Bx+Clnx shows good R square values. Activation entropy, enthalpy, and heat capacity change can be calculated from this fitting.

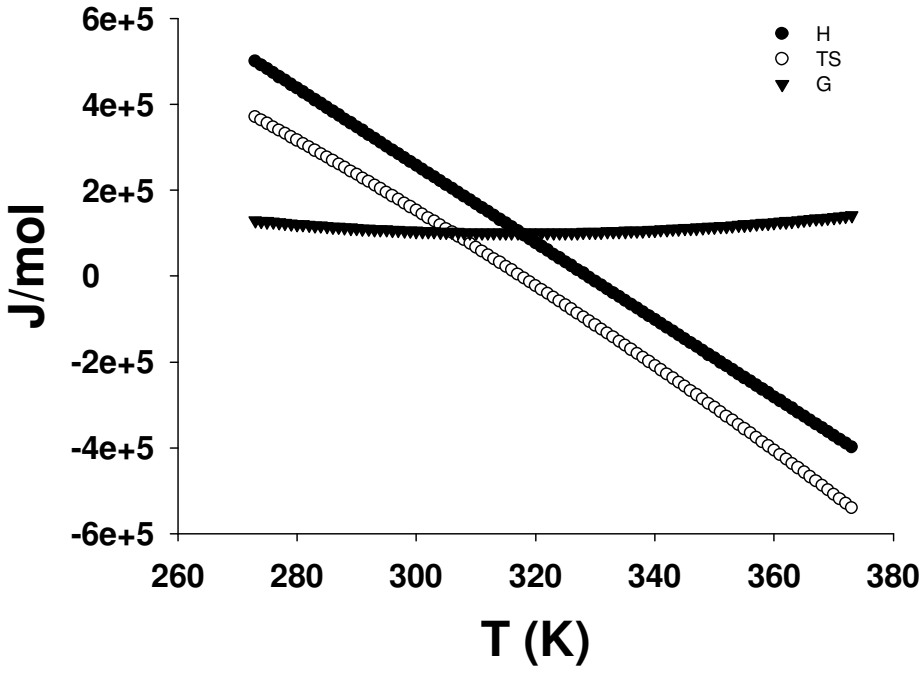

Figure 3.7. Activation enthalpy, activation entropy, and activation free energy of 10 mg/mL PNIPAM solution under different temperature.

PNIPAM collapse therefore the heat capacity change is negative during collapse process. Basically, large negative change of heat capacity, large positive enthalpy change and large positive entropy change indicates the formation of hydrophobic interaction. Trends of activation free energy, enthalpy and entropy at different temperature were calculated by eq 2 and eq 3 (Figure 3.7). Both the activation enthalpy and entropy decrease as temperature goes higher. This trend is cause by the negative value of heat capacity change and its temperature dependence is similar as observed in the protein folding process.[117,121] The entropy of desolvation of hydrophobic residue are larger at low temperature and decrease strongly as temperature increased,[126-127] this phenomenon agree with the result observed here as PNIPAM collapse is a process of desolvation.

This is the first example showing the temperature dependent behavior of PNIPAM collapse which resembles the refolding of protein from cold denaturation is also similar to the protein folding process of heat denaturation.[117] The result here indicates that the mechanisms of cold denaturation and heat denaturation might also be similar.

Effect of Salts. Specific ions effects on the thermodynamics of PNIPAM collapse have been shown in our previous study by the measurement of LCST change with different salts and different concentrations.[44] The salt effects on PNIPAN collapse kinetics are studied here by our new platform. Two salts are chosen, chloride, a weak kosmotrope and thiocyanate, a chaotrope. Chloride is in the middle of the Hofmeister series and the mechanisms of chloride effect on the PNIPAM LCST are similar to chaotrope[44] while in Pegram and Record's work,[128] chloride is a neutral but slightly

excluded from protein-water interface anion, therefore it could be seen as kosmotrope as well. There are two reasons for studying these two salts; first, these two salts change the LCST of PNIPAM in two different ways: chloride lowers the LCST of PNIPAM about 2 degrees and thiocyanate increases the LCST of PNIPAM about 0.9 degree at the concentration being used (0.2 M).[44] Secondly, the underlying mechanisms of these two salts on the LCST of PNIPAM are different. Both salts change LCST of PNIPAM by direct binding to PNIPAM and by increasing surface tension of water/hydrophobic interface of PNIPAM but; but the extent of these two mechanisms are different for these two salts. Chloride changes the LCST of PNIPAM mostly by increasing the surface tension of the water/hydrophobic interface, the direct binding is not obvious. Thiocyanate changes the LCST of PNIPAM by both the surface tension mechanism and the direct binding mechanism. It is known that surface tension mechanism lowers LCST of PNIPAM and direct binding mechanism increases LCST of PNIPAM.[44] By studying the PNIPAM collapse kinetics with these two salts, we are able to understand the effect of these two mechanisms to kinetics of PNIPAM collapse.

As shown in Figure 3.4, the kinetics of PNIPAM collapse was fastened in the presence of chloride under series of different temperatures. PNIPAM collapse kinetics with thiocyanate were similar to the kinetics of collapse without salts. All the collapse rates versus temperatures showed same pattern that the rate increment is larger at lower temperature region and become smaller at elevated temperature region and all collapses showed non-Arrhenius behavior while the curvatures are a little but different (Figure 3.5.). The kinetics of PNIPAM collapse with chloride showed that surface tension

mechanism increases PNIPAM collapse rate since the direct binding mechanism is weak in chloride solution.[44] Kinetics of PNIPAM collapse with thiocyanate indicates direct binding mechanism and surface tension mechanism completely counter balance each other therefore the overall kinetics appears similar in behavior to the PNIPAM collapse without salts.

Figure 3.6 shows the Eyring plots of the PNIPAM collapse with chloride and thiocyanate. The collapse with chloride showed a shift to higher temperature while collapse with thiocyanate showed different curvature. Shift of chloride line might be contributed by surface tension increment during collapse and curvature difference in thiocyanate comes from competition of the two mechanisms during collapse. The thermodynamic parameters of the PNIPAM collapse with 0.2 M chloride are 30~40% smaller compared with the PNIPAM water solution (Table 3.1). It is known that kosmotropes have salting-out effect on protein[129] which lower protein solubility and also lower the LCST of PNIPAM. Smaller value of enthalpy change of activation at 298.15 K indicates that the PNIPAM faces a smaller enthalpic barrier during collapse. Chloride increases surface tension of the water/hydrophobic interface around PNIPAM (therefore increase hydrophobic interaction) and makes PNIPAM undergo its phase transition easier. Increasing surface tension at interface reduced activation enthalpy of PNIPAM collapse by destabilizing hydrophobic hydration around PNIPAM hydrophobic surface.

Smaller heat capacity change (Table 3.1) in the presence of chloride indicates fewer iceberg water structures were released at transition state. Stronger hydrophobic interaction caused by chloride reduced hydrophobic residues exposed to water in both

Table 3.1.Themodynamic parameters of PNIPAM collapse in different conditions

	$\Delta H^{o\ddagger}$ (kJ/mol)	$\Delta S^{o\ddagger}$ (J/mol · K)	$\Delta C_p^{\ddagger}$ (kJ/mol · K)
PNIPAM(10 mg/ml)	274.3 ±2.6	565.5 ±22.6	-9.0 ±0.2
w/ 0.2 M NaCl	184.4 ±28.1	313.4 ±92.4	-6.4 ±1.4
w/ 0.2m NaSCN	347.8 ±21.5	835.9 ±68.8	-13.0 ±0.9

random coil state and transition state. The structure of the PNIPAM at transition state was less affected because less interaction with salts presented in the partial collapse structure. Binding of the thiocyanate on PNIPAM stabilized PNIPAM in the random coil configuration in water, therefore increases solubility and raises the LCST of PNIPAM. Increasing surface tension of the water/hydrophobic interface destabilizes hydrophobic hydration of the PNIPAM and this mechanism lowers LCST. 0.9 degree of LCST increment by thiocyanate addition indicates the direct binding dominates the thermodynamics at this condition. The entropy, enthalpy, and heat capacity change of activation at standard condition are 1.2~1.5 times larger than PNIPAM aqueous solution (Table 1) is the result after compensation of these two mechanisms. According to the result in the chloride study, increasing surface tension reduces thermodynamic parameters of the PNIPAM collapse. Larger values of thermodynamic parameters in the presence of thiocyanate imply that direct binding mechanism increases the thermodynamic parameters and the dominant factor in 0.2 M thiocyanate solution in thermodynamic aspect is direct binding mechanism. These thermodynamic parameters obtained from kinetics data fitting are in agreement with thermodynamic measurements of LCST trend of PNIPAM where the overall LCST increased which is the result of direct binding mechanism as well.

Larger heat capacity change might indicate more hydrophobic residues exposed to water in the coil state in the presence of thiocyanate (more water iceberg disappear after collapse cause larger heat capacity change). Although thiocyanate also affects the structure at transition state, but the structure change of transition state is smaller due to

less interaction between thiocyanate and the PNIPAM at transition state. Binding of thiocyanate to the amide group of PNIPAM stabilized the PNIPAM structure and let it become more soluble in water therefore more hydrophobic residues are able to be exposed to water in the presence of thiocyanate. Higher enthalpy value indicates larger enthalpic barrier. It is known that chaotrope act to destabilize aggregation of hydrophobic solute particles and this factor may also cause less hydrophobic aggregation in random coil state. All the thermodynamic parameters are in the same order as the study of the Hofmeister effects on kinetics stability of protein.[129]

Thiocyanate does not change the kinetics of PNIPAM collapse significantly but it varies thermodynamic parameters a lot which reveals the fact that surface tension and direct binding mechanisms contribute differently to thermodynamics and kinetics. Thermodynamically, direct binding is the dominant factor in the presence of 0.2 M thiocyanate, the results is shown both in increased LCST and increased thermodynamic parameters. Direct binding and increase surface tension contribute equally to kinetics but in different directions, one slows the collapse process and one fastens the collapse process, therefore the collapse rate is almost the same with 0.2 M thiocyanate in solution and without salts.

3.5.Conclusions

We have shown that this novel microfluidic device which combines a temperature jump and a continuous flow method is suitable to measure the kinetics of PNIPAM collapse. Series of temperature jumps and the non-Arrhenius behavior was

first shown in this article. Heat transfer issue was overcome by the small volume of the sample needed in the capillary tube. The rate of the PNIPAM collapse measured by this device is in good agreement with the previously reported single PNIPAM collapse.

The effects of salts on the kinetics of PNIPAM collapse was first shown in this study. The thermodynamics parameters can be calculated form kinetics parameters by using the transition state theory. The effects of salts on thermodynamic parameters such as activation free energy, activation enthalpy and activation entropy correlates well with the change of the LCST in our previous report. Chloride lowers the LCST of PNIPAM, decrease thermodynamic parameters of the PNIPAM collapse in the transition state by reducing the hydrophobic surface exposed to water; thiocyanate raises the LCST of PNIPAM and increases the thermodynamic parameters of the PNIPAM collapse by increasing the hydrophobic surface exposed to water.

Accurate measurement of polymer collapse or protein folding kinetics in millisecond range by this new device may provide further insight to the protein folding in the future.

CHAPTER IV

THE EFFECTS OF CHAIN LENGTH ON KINETICS AND THERMODYNAMICS OF ELP COLLAPSE ABOVE LCST: HYDROPHOBIC INTERACTIONS

4.1. Synopsis

The kinetics of elastin-like polypeptides (ELPs) was investigated by a novel T-jump continuous flow device. The hydrophobic collapse of ELPs composed of the same sequence but different chain length was triggered by different temperature jumps across the lower critical solution temperatures (LCST) of ELPs. Non-Arrhenius behaviors were found in all ELPs and thermodynamics parameters could be obtained by utilizing transition state theory. Activation parameters calculated from kinetics parameters showed convergence of T_S and T_H. The convergences were shown for the first time for the activation parameters. The residue contribution and hydrophobic interaction components in ELPs collapse could be separated from the observed values by using T_S and T_H. The negative $\Delta S^{\circ\ddagger}_{res}$ values and negative $\Delta H^{\circ\ddagger}_{res}$ values calculated reveal the fact that the backbone residue contributions enthalpically favor collapse and entropically oppose collapse. The positive $\Delta S^{\circ\ddagger}_{hyd}$ and $\Delta H^{\circ\ddagger}_{hyd}$ values indicate the collapse is driven entropically by hydrophobic interactions with an enthalpic barrier. Intramolecular hydrophobic interactions and intermolecular hydrophobic interactions could also be extracted from overall hydrophobic interactions. Parameters involving single ELP chains such as residue contributions and intramolecular hydrophobic interactions were in the same order as the protein folding case. This is the first time that each component in ELP

collapse has been studied separately and ELPs show great potential to be studied for further understanding of protein folding.

4.2. Introduction

Hydrophobic interactions are thought to be one of the main factors dominant in the protein folding process.[52] Due to the complex nature of protein, it is hard to extract hydrophobic interaction components in protein folding from other contributions such as polar group interactions and protein backbone contributions. Simples model are required to eliminate polar groups and be able to extract backbone contributions from the rest, thereby systematically studying the role of hydrophobic interactions in protein folding. Furthermore, the understanding of hydrophobic interactions in cold denaturation of proteins is more indistinct compared to its understanding in heat denatureation. Cold denaturation is observed for the molten globule state of proteins[130-131] and the cold denature temperature is typically estimated to be20 K or more below the freezing point of water.[53] Therefore, denaturants[54] and pH conditions[56] are required to study the cold denatureation of protein.

Elastin-like polypeptides (ELPs) are biopolymers comprised of a repetitive pentapeptide motive, Val-Pro-Gly-Xaa-Gly, where the guest residue, Xaa can be any amino acid expect Pro. ELPs undergo an inverse temperature transition[19-26] in which they are in disordered random coiled states in solution below the lower critical solution temperature (LCST) and are fully hydrated by hydrophobic hydration. On the contrary, when the temperature is raised above the LCST, ELPs hydrophobically collapse and

assemble into a phase separated state. The former step resembles cold denaturation of protein. The kinetics of the latter step, the formation of an aqueous two-phase system[27-30], had been studied by our group[31] using a temperature gradient apparatus while the former step, kinetics of hydrophobic folding, was never studied.

ELPs are good candidates for the study of cold denatureation of protein and the hydrophobic interactions occurring during this process because they show an inverse temperature transition and their sequence and chain length can be precisely controlled by recombinant synthesis.[57-58] Amino acids with polar group side chains can be avoid to eliminate the polar group component during collapse and chain length can be controled precisely to extract length related backbone contributions. Here, a set a ELPs with the same composition, wild type $V_5A_2G_3$ (which means 50 percent of the guest residues are valine, 20 percent of the guest residues are alanine and 30 percent of the guest residues are glycine) was used. The chain length is the variable amongst the four ELPs; I-30, I-60, I-120 and I-330 were used which means there are 30, 60 120 and 330 penta amino acids in each ELP respectively.

4.3. Experimental

ELP Preparation. The pET plasmids employed here were constructed by recursive directional ligation as previously described.[57] The plasmids were expressed in BLR/DE3 *E. coli* in high growth media, TBdry, with ampicillin for 24 h. Purification of the ELPs was done by sonication of the cells followed by a series of inverse transition cycling (ITC) steps. For example, one round of ITC was carried out by centrifugation at

10000g at 50 °C by adding 1 M NaCl (the temperature and NaCl concentration varies with ELPs: for an ELP with a higher LCST, higher temperature and more concentrated NaCl is required). The pellets (containing ELPs) were then dissolved in phosphate buffer (10 mM, pH 6.9, 4°C), and the remaining cellular debris was removed by centrifugation at 10000g. Typically, two rounds of ITC were needed to remove impurities. The concentrations of the purified ELPs solutions were determined by measuring the absorbance at 280 nm (ε = 5690 M^{-1} cm^{-1}). After purification by ITC, samples were dialyzed against purified water (NANOpure Ultrapure Water System, Barnstead, Dubuque, IA) with a minimum resistivity of 18 MΩ· cm to remove residual salts. Finally, the samples were lyophilized and stored at -80 °C until use.

Kinetics Measurement. A novel T-jump device was utilized to measure the kinetics of ELPs collapse triggered by different temperatures. A cover glass (22 × 22 mm) acting as both sample stage and heat conductor was mounted on top of two parallel brass tubes. Stainless steel sheath heaters were placed inside the brass tubes and connected to a variable autotransformer to control the temperature.

Square capillary tubes (0.1 × 0.1 mm) were fixed on a cover glass and connected to a plastic tube by capillary wax. The plastic tube was connected to a peristaltic pump tube mounted on a peristaltic pump by which the flow of the ELPs solution was controlled. Light scattering from polymer solutions was monitored via a CCD camera using dark field optics under an inverted microscope. The distance between the T-jump point and the light scattering point at which the ELPs were considered to be collapsed was measured and it can be converted into time based on the calculation with the flow rate

and the dimensions of the capillary.

4.4. Results

LCST of ELPs. It has been shown that the LCST of ELPs was determined by the sequence, hydrophobicity and mole fraction of guest residues at the fourth position, concentration and the chain length of the ELPs.[58,132-134] Both the chain length and concentration vary in our case, where the monomer concentration was kept constant therefore making the concentration of ELPs with longer chain length lower and the concentration of shorter ELPs higher. It is known that ELPs with longer chain length collapse at lower temperature and ELPs with higher concentration also collapse at lower temperature. According to Meyer and Chilkoti's study, the transition temperature of ELPs with the same sequence have an inverse relationship with the chain length and a logarithmic relationship with the reciprocal of the concentration.[58] The dominant factor would be the chain length because the concentration factor is not profound after logarithm. The trend of LCST for the four ELPs used in this experiment agrees with Meyer and Chilkoti's equation in their quantification study as shown in Figure 4.1. After the combination of the chain length and concentrations, I-330 showed the lowest LCST followed by I-120 and I-60 while I-30 had the highest LCST among the four ELPs.

Kinetics of ELPs Collapse. The four ELPs lines spread out in the rate versus temperature figure due to the LCST differences among the ELPs as shown in Figure 4.2. All four ELPs showed similar collapse behavior in that the collapse rate increased as temperature went higher. The rate increment was larger at lower temperatures and

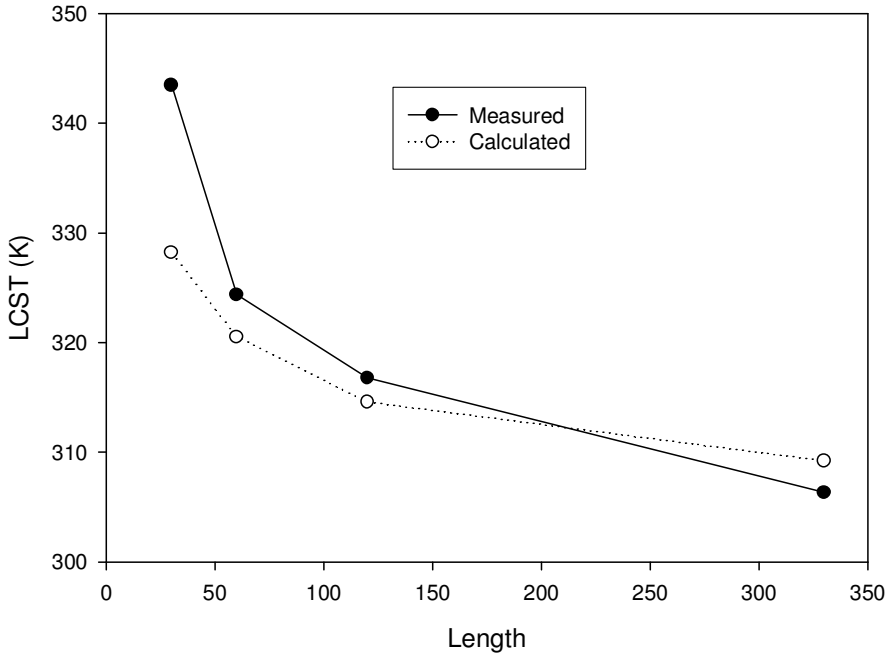

Figure 4.1. The LCST of ELPs with different chain lengths measured and calculated.

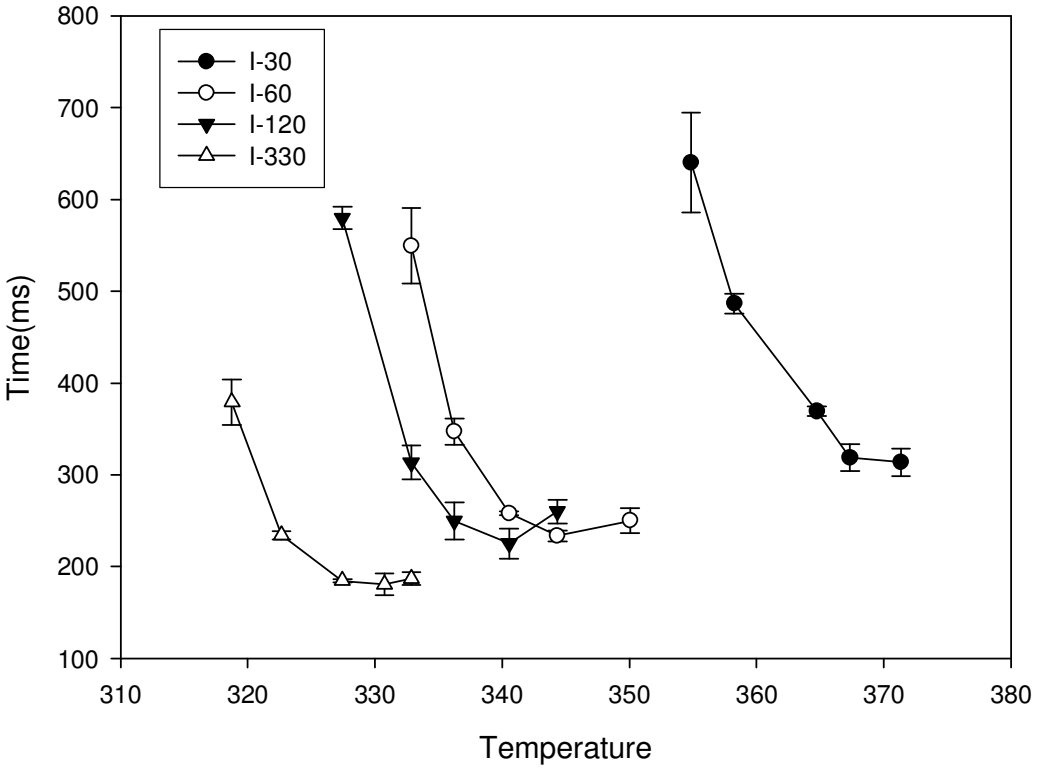

Figure 4.2. Collapse rate of ELPs triggered by different temperature shows ELPs with higher LCST collapse slower under the same temperature.

became smaller at higher temperatures. The rate versus temperature plots go flat and even decrease at high temperatures far away from the LCST of ELPs. This behavior is similarly observed in protein folding and in the thermal responsive polymer, Poly(N-isopropyl acrylamide) (PNIPAM) experiment.[135] When we utilized an Arrhenius plot (ln(k) versus 1/T, data not shown), we found non-Arrhenius behavior and this was shown for the first time as ELPs collapse triggered by series of temperature jumps. This non-Arrhenius behavior is similar to protein folding.[120-121,136] The curve was linear at lower temperatures and derived from linear at higher temperatures, which indicates the collapse was dominated by enthalpy at lower temperature and entropy takes over at high temperatures.[122-123]

Figure 4.3 shows the rate versus temperature differences from LCST of individual ELPs. By plotting rate/temperature in this way we are able to eliminate the difference that comes from the intrinsic LCST difference. ELP I-60, I-120, and I-330 showed almost the same temperature dependence while ELP I-30 showed similar curvature at about five degrees higher and about 150 ms slower. Although the monomer concentrations were kept the same for all ELP samples, the chain length varies. The weak trend of collapse rate in ELPs indicates the collapse rate is mainly determined by the monomer concentrations, and the chain length has only minor contribution.

Thermodynamics Study of ELPs Collapse. There is not much literature to be found dealing with the kinetics of polypeptide collapse involving multiple chain aggregation. We found that the kinetic parameters could be fit nicely with transition

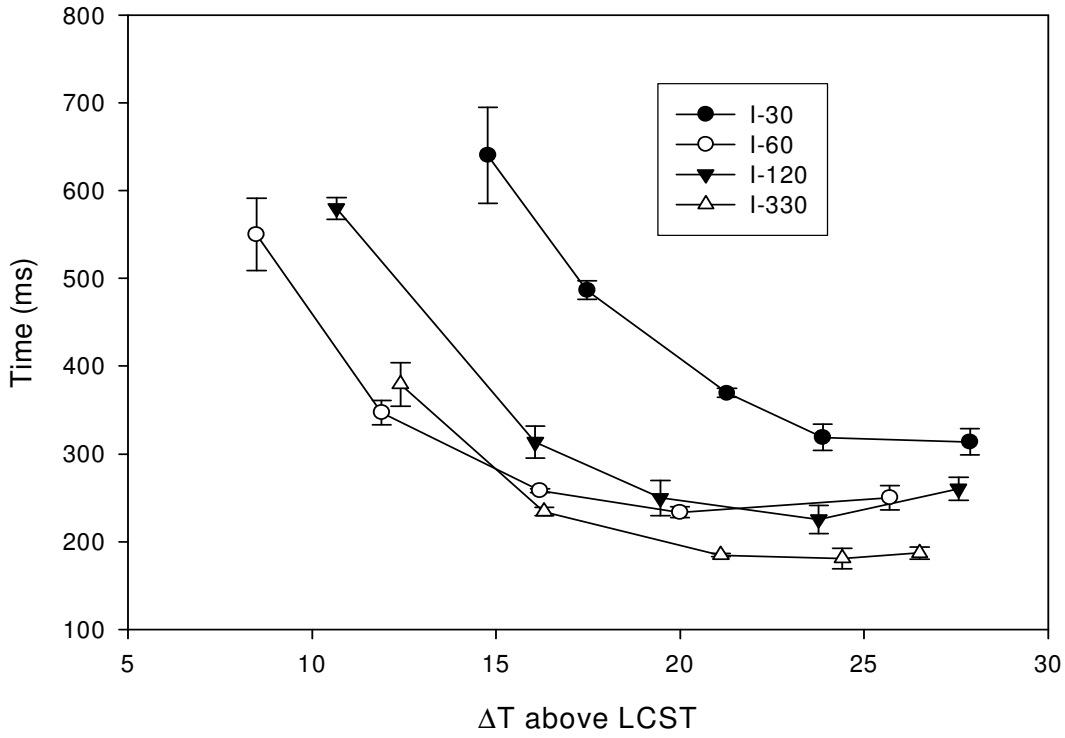

Figure 4.3. Collapse rate versus temperature above LCST shows weak tendency toward chain length.

state theory. Previously, our PNIPAM data[135] showed that measurements are due to formations of PNIPAM particles formed caused by PNIPAM collapse involving multiple chain aggregation, not the growth of PNIPAM particles after collapse caused by particle aggregation, which is why the data can be fit by transition state theory equations used in protein unfolding study. Due to similar time scales and good fitting, we believe that is the same case here. The measurements are due to formation of ELP particles formed due to ELPs collapse involving multiple chain aggregation, not the growth of ELP particles after collapse due to particle aggregations. This was proven to be on the order of hundreds of seconds.[31] By fitting kinetic parameters with an Eyring plot, which is derived from Arrhenious equation, we are able to get the thermodynamic parameters involved in the collapse process. This method is similar to that used in protein denaturation studies.[117-118]

To learn the thermodynamic characteristics of ELP collapse, we fit our data with transition-state theory according to the Eyring equation

$$k = \frac{\kappa k_b T}{h} \exp\left[-\left(\frac{\Delta G^{0\ddagger}}{RT} \right) \right] \qquad (1)$$

where k_b is Boltzmann constant, h is Plank's constant, R is the gas constant. κ is the transmission factor with an upper limit of 1.

Since G = H-TS and activation enthalpy and activation entropy are temperature dependent as

$$\Delta S^{\ddagger}(T) = \Delta S^{\ddagger}(T_0) + \Delta C_p^{\ddagger} \ln(T / T_0) \qquad (2)$$

$$\Delta H^{\ddagger}(T) = \Delta H^{\ddagger}(T_0) + \Delta C_p^{\ddagger}(T - T_0) \qquad (3)$$

Combining these three equations we get

$$\ln\frac{k}{T} = \ln\frac{\kappa k_B}{h} + \frac{\Delta S^{\ddagger}(T_0)}{R} - \frac{\Delta C_p^{\ddagger}}{R} - \frac{\Delta C_p^{\ddagger}}{R}\ln T_0 + \left(\frac{\Delta C_p^{\ddagger}(T_0)}{R} - \frac{\Delta H^{\ddagger}(T_0)}{R}\right)\frac{1}{T} + \left(-\frac{\Delta C_p^{\ddagger}}{R}\right)\ln\frac{1}{T} \qquad (4)$$

Consequently, by plotting ln(k/T) against 1/T(Eyring plot), we are able to get heat capacity change ($\Delta C_p^{\ddagger}$), activation entropy ($\Delta S^{\circ\ddagger}_{\text{obs}}$) and activation enthalpy ($\Delta H^{\circ\ddagger}_{\text{obs}}$).[2,118,121,137] The only assumption made is the heat capacity change is constant in the temperature range of interest.

All four ELPs showed negative values in heat capacity change of activation which is in agreement with the fact that there are more clathrate-like water molecules around hydrophobic surfaces of ELPs[138] at extended state and certain amounts of water molecules were excluded from the hydrophobic surface in the partially-collapsed transition state. The clathrate-like water molecules have limited orientation at lower temperatured and more orientations are available when the temperature goes higher. This contributes to the heat capacity because the energy in the system increases with temperature.[52,124-125]

As shown in Figure 4.4, heat capacity change of the activation correlates with the length of ELPs. Two kinds of contributions were found from the linear regression: a constant part and a length related part. A possible mechanism of ELP phase transition was proposed such that when the temperature is increased the peptides undergo a conformation change from more random chains into β-turn-like structures with

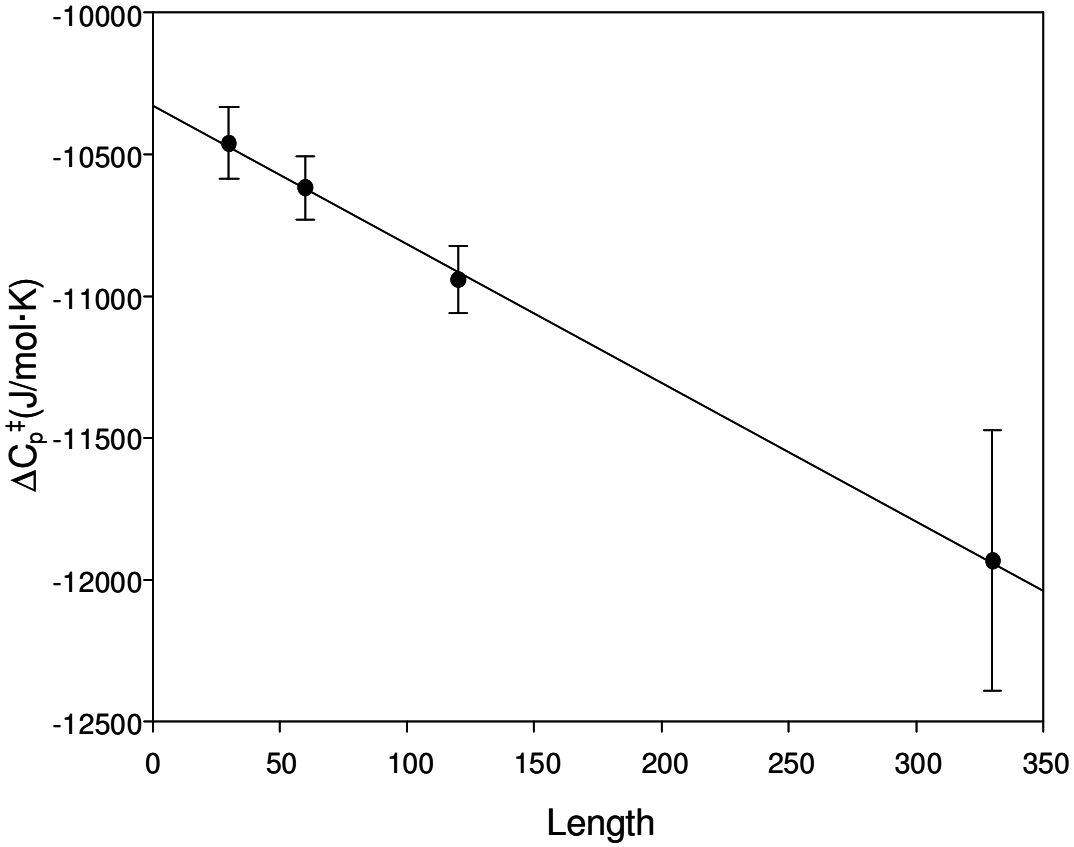

Fugure 4.4. The plot of heat capacity change of activation against length shows a length related (slope) part of heat capacity change and a constant part of heat capacity change (intercept value). Length related part is considered to be intramolecular hydrophobic interaction and constant part is considered to be intermolecular hydrophobic interactions.

hydrophobic groups exposed to solvent, which induces intermolecular association.[139] Therefore, the constant contribution comes from the intermolecular association of ELPs because the monomer concentrations were kept the same in all ELPs solutions, and the possibility of intermolecular association should be the same in the same confined volume. Water molecules were excluded from the hydrophobic surface of ELPs as intermolecular association proceeded, and the number of clathrate-like water molecules decreased as the hydrophobic surface of ELPs was brought together during collapse. Therefore, the heat capacity contributed by clathrate-like water decreased, and as a result, the heat capacity change is a negative value.

The length-related component in heat capacity change of the activation could be intramolecular hydrophobic association. β-Spiral structure is the result of optimized intramolecular hydrophobic contacts,[19] and water molecules were excluded from ELP surfaces in the formation of β-Spiral structures. The water molecules excluded from the hydrophobic surface of ELPs during the formation of β-Spiral would be proportioned to the length of ELPs, as more water molecules would be excluded from hydrophobic surfaces for longer ELPs compare to shorter ELP chains. Therefore, the length related component in heat capacity change of the activation is considered to be an intramolecular hydrophobic association component.

The $\Delta S^{\circ\ddagger}_{obs}$ and $\Delta H^{\circ\ddagger}_{obs}$ calculated from kinetic parameters are one order larger than the values obtained in small peptides studies[118,136] which involved single peptide chain folding. In our system, ELPs collapse involving multichain aggregation so higher values are expected and will be discussed later. Both observed entropy and enthalpy of

activation under standard state (25 °C) showed negative correlation with chain length of ELPs as shown in Table 4.1 On the other hand, the observed entropy and enthalpy of activation under standard state correlate with concentration of ELPs. Observed enthalpy and entropy of activation shows a linear relationship and we will discuss later that observed thermodynamic parameters are composed of residue contribution and intermolecular/intramolecular hydrophobic interaction contributions. Some of these (residue and intramolecular hydrophobic interaction contributions) are proportion to the length of ELPs and some (intermolecular hydrophobic interactions) only relate to concentration of the ELP monomers and therefore are constant in all ELPs. Since the composition and relationship are the same in observed entropy of activation and observed enthalpy of activation, a linear relationship between these two is expected.

If we utilize equations 2 and 3 to calculate entropy and enthalpy of activation at LCST for each ELP at which the collapse process starts we obtain the same trend as the previous study of ELPs by DSC in which the hydrophobicity of ELPs was controlled.[134] The entropy and enthalpy change increased as the hydrophobicity of ELPs increased, accompany by the decrease of the LCST.

4.5. Discussion

Convergence of T_S and T_H. Back in the late 1970's, Privalov noted the denaturational enthalpy and entropy changes for a series of globular proteins extrapolate to a common value around 110 °C (per unit residue).[140] This is also the temperature at which the entropy of transferring a hydrocarbon from pure liquid to water is zero.[141] The

explanation for this phenomenon is that at around 110 °C, hydrophobic interaction contributions to entropy change are zero. The conformational entropy upon unfolding is similar for those proteins studied by Privalov.[142] On the other hand, the temperature at which the minimum solubility occurs ($\Delta H=0$) for hydrocarbons is at around room temperature[143] while the temperature of unfolding enthalpy changes converge around 110 °C (T_H).[144] Some assumptions were made and mathematical methods have been used to prove T_H and T_S should be similar for protein unfolding.[142,145-146] Polar interactions were considered in protein unfolding[147-148] and could be used to explain the shift of T_H from the liquid hydrocarbon model to protein unfolding,[149] but the difference of T_H in the liquid hydrocarbon model and in protein unfolding reveal that T_H are not necessary be the same.

Convergences of entropy and enthalpy change of activation were also found in this study. A plot of activation entropy change per residue versus temperature showed a convergence close to 340 K and a plot of activation enthalpy change per residue versus temperature showed a convergence close to 350 K. Plots of unit change of activation entropy and enthalpy against unit change of heat capacity at a single temperature could be applied to get the T_S and T_H from the slope, as shown in Figure 4.5 and 4.6, in order to remove possible effects of a temperature dependence of heat capacity change.[150] The ELP I-30 showed a larger error bar due to the fact that the LCST of this ELP is more than 20 degrees higher than the other three and some of the temperature jumps are close to the boiling point of water. The intercept values in the plots correspond to the

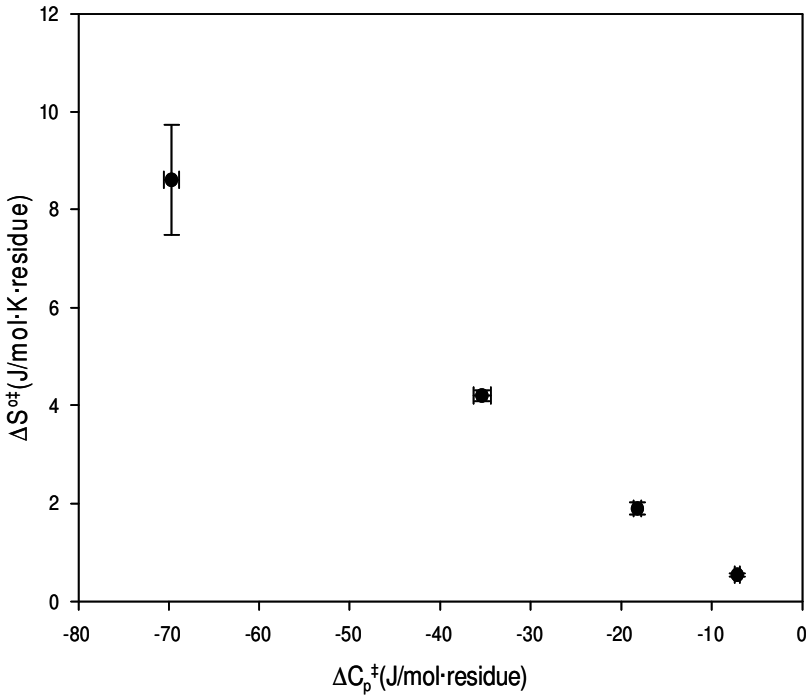

Figure 4.5. A linear correlation between entropy change of activation versus heat capacity change of activation at 25 ℃ among 4 ELPs enables us to calculate the T_s from the slope. $\Delta S=\Delta S^*+\Delta C_p \ln(T/T_S^*)$ The intercept corresponds to a process involving no change in heat capacity and can be seen as the nonhydrophobic contribution to the ΔS.

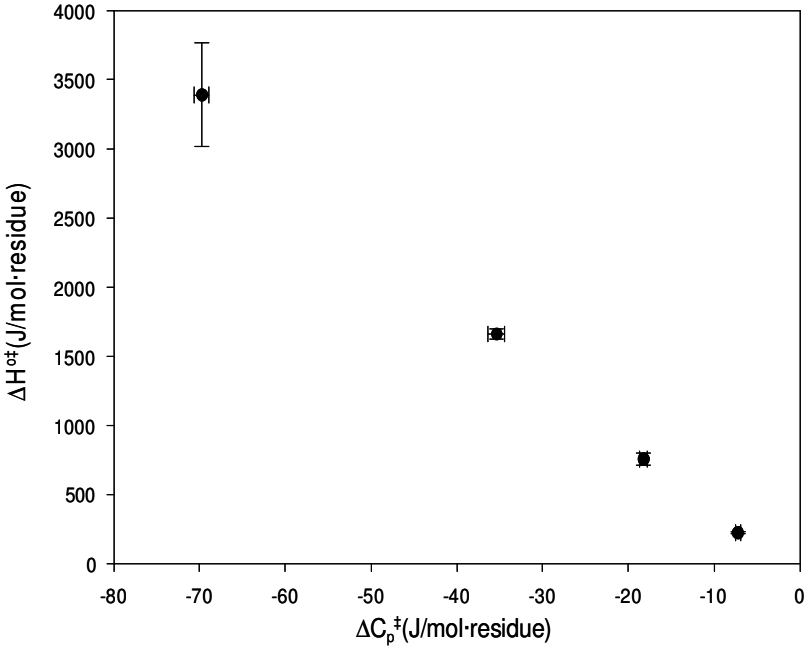

Figure 4.6. A linear correlation between enthalpy change of activation versus heat capacity change of activation at 25 ℃ among 4 ELPs enables us to calculate the T_H from the slope. $\Delta H=\Delta H^*+\Delta C_p(T-T_H^*)$ The intercept corresponds to a process involving no change in heat capacity and can be seen as the nonhydrophobic contribution to the ΔH.

contribution with no change in heat capacity and can be seen as nonhydrophobic contributions and will be discussed later.T_S (339.4 K) and T_H (349.0 K) are obtained from the slopes which are $\ln(T/T_S)$ and $T-T_H$ as shown in equation 2 and 3. T_S and T_H found in this study are quite different from the T_S and T_H values found in the protein unfolding experiment[140] and in the liquid hydrocarbon model.[151] Several possible reasons may cause this difference. Firstly, in the protein unfolding experiment and in the liquid hydrocarbon model, the processes are to transfer a nonpolar substance from a nonpolar environment to aqueous solution. In our study, we focus on the process of ELPs hydrophobic collapse, which is a process removing a nonpolar substance from an aqueous environment to a nonpolar environment. Secondly, both in the protein unfolding and the transferring hydrocarbon case, thermodynamics was studied. The thermodynamic parameters like ΔC_p , ΔH and ΔS calculated are the difference between initial state and the final state. Kinetics was studied in our case, and transition state theory was applied to calculate thermodynamics parameters from kinetics parameters. Thermodynamic parameters like $\Delta C_p^{\ddagger}$, $\Delta H^{\circ\ddagger}_{\text{obs}}$ and $\Delta S^{\circ\ddagger}_{\text{obs}}$ are activation parameters, which is the difference between initial state and the transition state. This is the major difference in our study compared to previous studies. Thirdly, in the protein unfolding study, the process being studied is the heat denaturation of protein across upper critical solution temperature. In the ELPs study, collapse of ELPs across lower critical solution temperature (cold denaturation) was studied. Therefore, not only is the direction different, but the critical temperatures studied are also different. Even for the

protein unfolding and the transferring hydrocarbon experiments, the T_H is quite different. As a result of these differences, it is reasonable to get a different T_S and T_H in our study.

Hydrophobic Interaction and Residue Contribution. If we assume the temperatures of convergence (T_S and T_H) are the temperatures at which hydrophobic interaction contributions are zero, as in the protein unfolding study, entropy and enthalpy change of activation contributed by hydrophobic interactions at different temperatures could be calculated by equation 2 and 3 by replacing T_0 with T_H in equation 2 and with T_S in equation 3.

Residue contributions of activation entropy, basically conformational contributions of ELPs backbone, could be obtained by two methods. First, by plotting $\Delta S^{o\ddagger}_{obs}$ against $\ln(T_S/T)$, since $\Delta S^{o\ddagger}_{obs}$ is composed of hydrophobic interaction contributions ($\Delta S^{o\ddagger}_{hyd}$) and residue contributions ($\Delta S^{o\ddagger}_{res}$) and $\Delta S^{o\ddagger}_{hyd}$ is 0 at T_S. Also, the equation $\Delta S^{o\ddagger}_{obs}(T) = \Delta S^{o\ddagger}_{obs}(T_S) + \Delta C_p{}^{o\ddagger} \ln(T/T_S)$ reveals that in plotting $\Delta S^{o\ddagger}_{obs}$ against $\ln(T_S/T)$, the intercept will be $\Delta S^{o\ddagger}_{obs}(T_S)$, that is $\Delta S^{o\ddagger}_{res}$.[151] The second method utilizes the intercept value in Figure 4.5, and as mentioned before, the intercept values in the plots correspond to the contribution with no change in heat capacity and can be seen as nonhydrophobic contributions. The intercept value is the unit residue contributions to the entropy change of activation. In order to get the residue contributions of the whole ELP chain, the number of residues in one ELP is used, 150 for ELP I-30, 300 for ELP I-60, 600 for ELP I-120 and 1650 for ELP I-330 (as mentioned, the numbers indicate the numbers of penta amino acid motif). The results are shown in the Table 3.1 together with

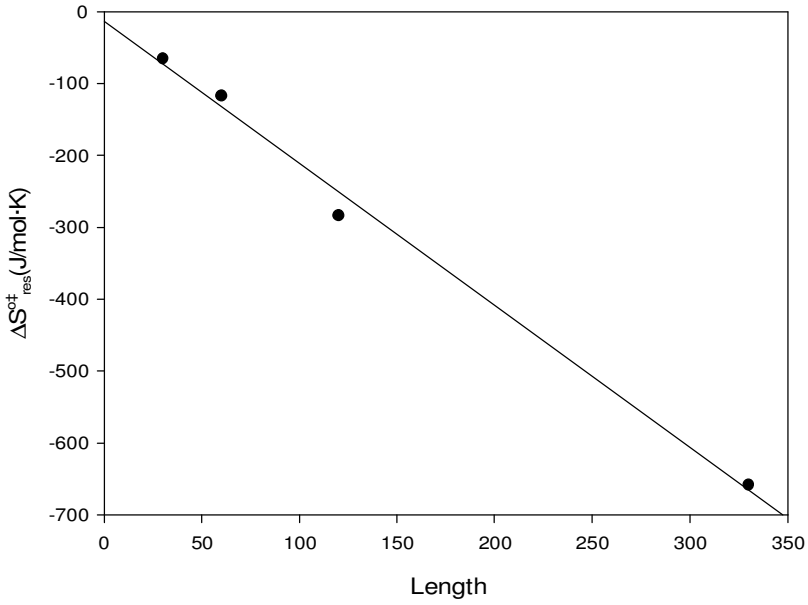

Figure 4.7. Entropy changes of activation contributed by ELPs residues show a linear correlation with chain length. The $\Delta S^{\ddagger}_{res}$ was obtained from the intercept of $\Delta S^{\ddagger}_{obs}$ versus ln(Ts/T) plot.

the intercept values of plotting $\Delta S^{\circ\ddagger}_{obs}$ against ln(T_S/T) for each ELP. As shown in Table, these two values are very close to each other, the differences are from 2 % to around 11 %. The matching of these values indicates that the assumption that convergent temperatures are the temperatures at which hydrophobic interaction contributions are zero is reasonable. Furthermore, the $\Delta S^{\circ\ddagger}_{res}$ values obtained for all four ELPs in both methods are negative values, which agree with the fact that at the transition state, the ELP structure is partially collapsed and therefore the entropy of the conformation is decreased. If we plot the intercept values in the $\Delta S^{\circ\ddagger}_{obs}$ against ln(T_S/T) plot for each ELP versus the length of the ELPs, we get a linear correlation (Figure 4.7.). Again, this linear correlation supports the assumption that the hydrophobic interactions of activation entropy are zero at T_S.

The same two methods are used to treat enthalpy change of activation of ELPs collapse to calculate residue contributions in enthalpy change of activation ($\Delta H^{\circ\ddagger}_{res}$). The intercept value in Figure 4.6 is multiplied by the numbers of residues for four ELPs and the intercept values in the $\Delta H^{\circ\ddagger}_{obs}$ against (T-T_H) plot. The results are shown is Table 4.1. The values obtained from the individual ELP plots agree with the values obtained from the intercept combining four ELPs (Figure 4.6., $\Delta H^{\circ\ddagger}_{obs}$ per residue versus $\Delta C_p^{\ddagger}$ per residue). A linear correlation also can be obtained by plotting the intercept values in the $\Delta H^{\circ\ddagger}_{obs}$ against (T-T_H) plot for each ELPs as shown in Figure 4.8.. This result supports the assumption that the hydrophobic interaction contributions to the enthalpy change of activation are zero at T_H.

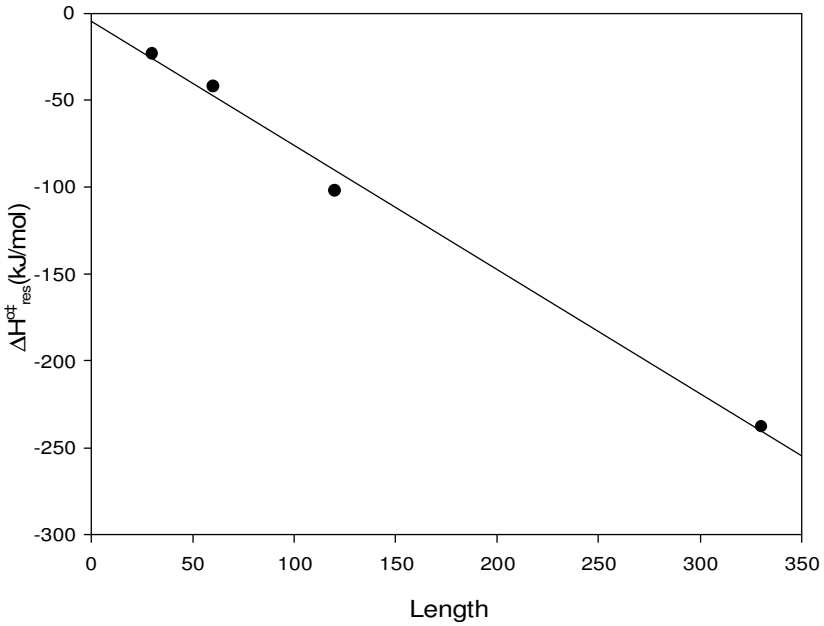

Figure 4.8. Enthalpy change of activation contributed by ELP residues shows a linear correlation with chain length. The $\Delta H^{\ddagger}_{res}$ was obtained from the intercept of $\Delta H^{\ddagger}_{obs}$ versus ($T-T_H$) plot.

The negative $\Delta S^{o\ddagger}_{res}$ values and negative values of $\Delta H^{o\ddagger}_{res}$ calculated reveal the fact that the backbone residue contributions enthalpically favor collapse and entropically oppose collapse and this agrees with the trend obtained in a previous study.[151]

Intramolecuar and Intermolecular Hydrophobic Interactions. As discussed, two components in heat capacity change of activation were found in the $\Delta C_p^{\ddagger}$ versus length plot. The constant component is thought to be heat capacity change due to intermolecular association, and length related component is thought to be intramolecular association, the formation of β-spiral. The percentages of intramolecular molecular hydrophobic interactions were estimated by multiplying the slope in Figure 4.4 with the lengths of each ELP and dividing by the observed heat capacity change. The results are shown in Table 4.2, and as can be seen in the table, the intramolecular hydrophobic interaction is small in shorter ELPs and becomes larger in longer ELPs. In ELP I-30, only 1.4 % of heat capacity change is due to intramolecular hydrophobic interactions, while most of the heat capacity change (98.6%) is from intermolecular association of ELPs. The contributions from intramolecular hydrophobic interactions increased as ELPs chains became longer. For the longest ELP used in this study, ELP I-330, the contribution of intramolecular hydrophobic interaction became 13.51%, which is about ten times larger than in ELP I-30.

$\Delta S^{o\ddagger}_{res}$ and $\Delta H^{o\ddagger}_{res}$ were calculated in the previous section by using T_S and T_H values and $\Delta S^{o\ddagger}_{obs}$ and $\Delta H^{o\ddagger}_{obs}$ were obtained by fitting kinetics data. Since $\Delta S^{o\ddagger}_{obs} = \Delta S^{o\ddagger}_{hyd} + \Delta S^{o\ddagger}_{res}$ and $\Delta H^{o\ddagger}_{obs} = \Delta H^{o\ddagger}_{hyd} + \Delta H^{o\ddagger}_{res}$, hydrophobic interaction

components could be acquired for all four ELPs as shown in Table 4.2. The contributions of inter and intramolecular hydrophobic interactions to the $\Delta S^{o\ddagger}_{hyd}$ and $\Delta H^{o\ddagger}_{hyd}$ can be obtained by multiplying $\Delta S^{o\ddagger}_{hyd}$ and $\Delta H^{o\ddagger}_{hyd}$ with the percentage calculated. The results are listed in Table 4.2. Although $\Delta S^{o\ddagger}_{hyd}$ and $\Delta H^{o\ddagger}_{hyd}$ are different for the four ELPs and the percentages are all different, the $\Delta S^{o\ddagger}_{hyd}$ and $\Delta H^{o\ddagger}_{hyd}$ that come from intermolecular hydrophobic interactions are surprisingly constant in all four ELPs which agrees with the fact that heat capacity change due to intermolecular hydrophobic interactions is constant in all four ELPs because constant monomer concentrations were used in the experiments. Furthermore, if we plot the intermolecular hydrophobic interaction components in $\Delta S^{o\ddagger}_{hyd}$ and $\Delta H^{o\ddagger}_{hyd}$ against the length of ELPs, linear regressions passing through zero are obtained. All these results support the assumptions that hydrophobic interaction contributions to the entropy chang of activation are zero at T_S and enthalpy contributions are zero at T_H.

On the other hand, another method can be applied to extract intermolecular and intramolecular hydrophobic interactions from overall hydrophobic interaction contributions. The overall hydrophobic interactions listed in Table 1 contain constant intermolecular hydrophobic interaction parts and length related intrarmolecular hydrophobic interaction parts. Plots of $\Delta S^{o\ddagger}_{hyd}$ and $\Delta H^{o\ddagger}_{hyd}$ against length showed a linear regression that agrees with the constant intermolecular hydrophobic interaction part and the length related intramolecular hydrophobic interaction part. (Figure 4.9 and 4.10). The length related values are listed in Table 4.2 as the slope values in each figure are

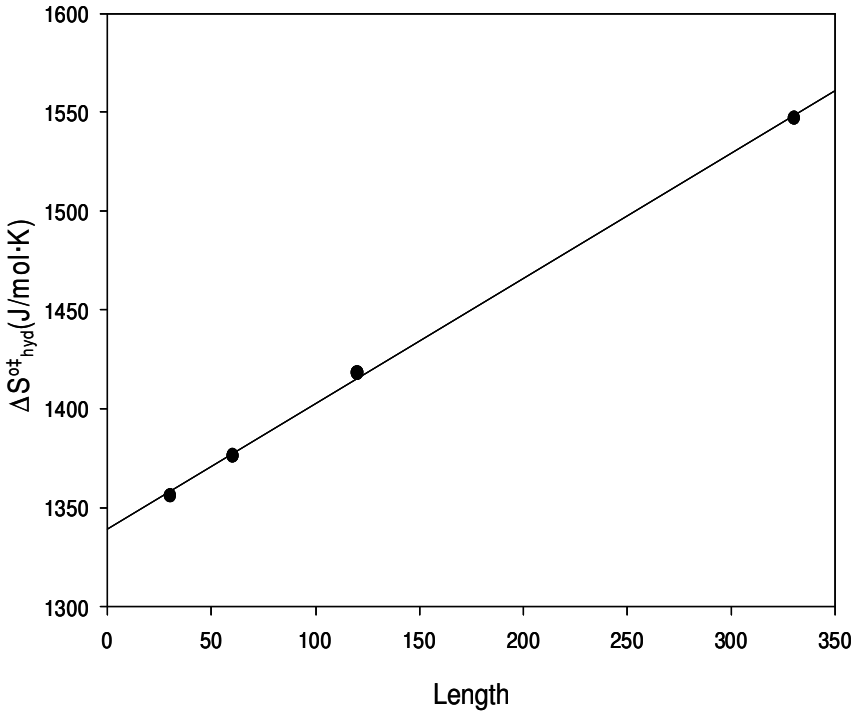

Figure 4.9. Entropy changes of activation contributed by hydrophobic interactions show a linear correlation with chain length. The constant part and the length related part can be separated from this figure.

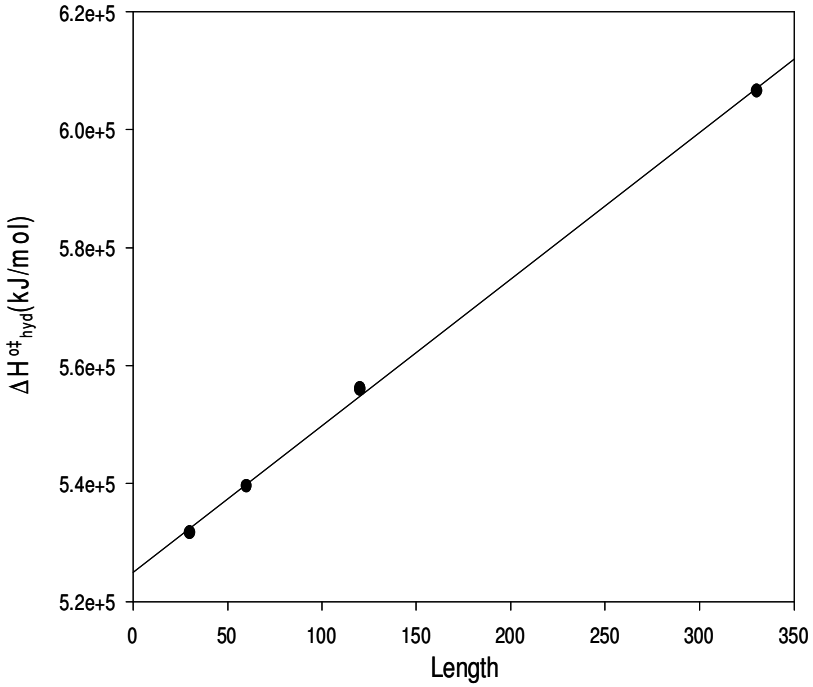

Figure 4.10. Enthalpy changes of activation contributed by hydrophobic interactions show a linear correlation with chain length. The constant part and the length related part can be separated from this figure.

multiplied by the n values of ELPs. The constant part is also listed in table as the intercept value in the figures. The values calculated by this method agree with the values obtained by percentages estimated from the heat capacity change value. The matching of values obtained from two different methods supports the assumption that the heat capacity and the hydrophobic interactions can be separated into intermolecular and intramolecular hydrophobic interactions.

Although the $\Delta S^{\circ\ddagger}_{obs}$ and $\Delta H^{\circ\ddagger}_{obs}$ calculated from kinetic parameters are one order larger than the values obtained in the small peptides study,[118,136] the $\Delta S^{\circ\ddagger}_{res}$, $\Delta H^{\circ\ddagger}_{res}$, $\Delta S^{\circ\ddagger}_{hyd}$, and $\Delta H^{\circ\ddagger}_{hyd}$ of intermolecular hydrophobic interactions, which involved only single ELP chains, are within the same order of magnitude as the peptide study involving single peptide folding. This fact shows that the larger values of $\Delta S^{\circ\ddagger}_{obs}$ and $\Delta H^{\circ\ddagger}_{obs}$ obtained in the ELP collapse study comes from multichain aggregation and agrees with previous assumptions.

Activation Energy Contributed by Backbone of ELPs. Observed activation energy can be estimated by $\Delta G=\Delta H-T\Delta S$ and the hydrophobic interaction components of activation energy could be calculated by $\Delta G=\Delta C_p[(T-T_H)-T\ln(T/T_S)]$. The difference between these two values is the contributions from the backbone of the ELPs, as showed in Figure 4.11. The values of backbone components are negative below about 362 K which means the backbone favors collapse as a result of a negative enthalpy change contribution from the backbone. As temperature goes higher, the backbone contributions

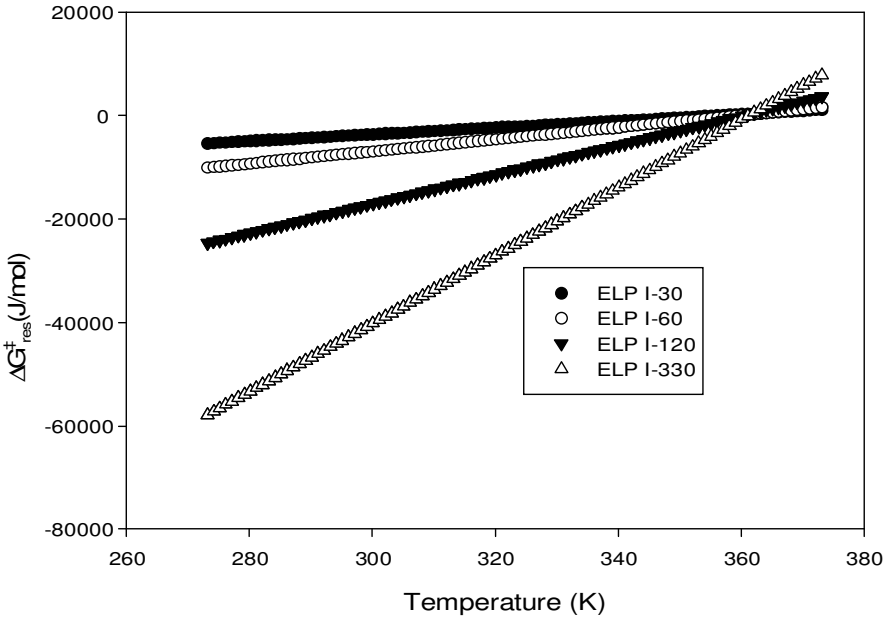

Figure 4.11. Activation energy of backbone residue contribution could be obtained from the difference between observed value ($\Delta G=\Delta H-T\Delta S$) and the hydrophobic interaction component ($\Delta G=\Delta C_p[(T-T_H)-T\ln(T/T_S)]$).

Table 4.1. Thermodynamic parameters of ELP collape

	$\Delta C_p^{\ddagger}$ (J/mol·K)	$\Delta S^{o\ddagger}_{obs}$ (J/mol·K)	$^{a}\Delta S^{o\ddagger}_{res}$ (J/mol·K)	$\Delta S^{o\ddagger}_{hyd}$ (J/mol·K)	$\Delta H^{o\ddagger}_{obs}$ (J/mol)	$^{a}\Delta H^{o\ddagger}_{res}$ (J/mol)	$\Delta H^{o\ddagger}_{hyd}$ (J/mol)
I-30	-10461.2	1291.3	-64.94	1356.2	508624.6	-23118	531742.7
I-60	-10617.3	1259.7	-116.73	1376.5	497732.6	-41946	539678.7
I-120	-10940.8	1135.4	-282.97	1418.4	454163.3	-101955	556118.3
I-330	-11934.0	889.6	-657.57	1547.2	369070.8	-237537	606607.8

a: the residue contributions calculated from the intercept of $\Delta S^{\ddagger}$ vs $\ln(T_S/T)$ and $\Delta H^{\ddagger}$ vs. $T-T_H$ for four ELPs individually.

Table 4.2. Individual contributions in the collapse process

	Intra	Inter	$\Delta H^{o\ddagger}_{hyd}$ (intra) J/mol	$\Delta H^{o\ddagger}_{hyd}$ (inter) J/mol	$\Delta S^{o\ddagger}_{hyd}$ (intra) J/mol · K	$\Delta S^{o\ddagger}_{hyd}$ (inter) J/mol · K
I-30	1.40%	98.6%	7452.34	524290.31	19.01	1337.21
I-60	2.76%	97.24%	14904.67	524773.98	38.01	1338.44
I-120	5.36%	94.64%	29809.35	526308.92	76.03	1342.35
I-330	13.51%	86.49%	81975.78	524632.02	209.08	1338.07

After multiplying the percentage calculated from heat capacity change data, hydrophobic interactions could be separated into constant intermolecular hydrophobic interaction terms and length related intramolecular hydrophobic interaction terms.

become positive. This agrees with the fact that the driving force of protein heat denaturation is the backbone entropy overcoming other the stability forces in the protein.

4.6.Conclusions

Here we showed the study of ELPs collapse kinetics studied by a novel T-Jump continuous flow device. The slower aqueous process involving the formation of two-phase system occurring in hundreds of seconds concurs along with collapse in thermodynamic study of ELPs, like a DSC measurement, was avoided in our system. A millisecond time scale was observed for collapse of ELPs which is in the same order of magnitude for the collapse of thermal responsive polymers. Kinetics of ELP collapse for four ELPs with same in composition but different chain length was studied and all showed non-Arrhenius behavior as triggered by different temperatures. Relative collapse rates were similar when discussing the collapse triggered by the same temperature above LCST of each ELP.

Activation parameters ($\Delta C_p^{\ddagger}$, $\Delta S^{\circ\ddagger}_{\text{obs}}$ and $\Delta H^{\circ\ddagger}_{\text{obs}}$) were calculated via transition state theory. Due to the unique system used in this study, the convergence temperatures of ELP collapse were first found and residue contributions ($\Delta S^{\circ\ddagger}_{\text{res}}$, $\Delta H^{\circ\ddagger}_{\text{res}}$) and hydrophobic interaction contributions ($\Delta S^{\circ\ddagger}_{\text{hyd}}$, $\Delta H^{\circ\ddagger}_{\text{hyd}}$) could be extracted from the overall observed values. Hydrophobic interaction components were further separated into inter and intramolecular hydrophobic interactions by utilizing the heat capacity change value. Parameters involving single ELP chains, such as residue contribution and

intramolecular hydrophobic interactions were on the same order as the protein folding case.

Therefore, utilizing a unique ELP system, hydrophobic contributions from intermolecular and intramolecular associations, and residue contributions could be study individually. The polar group interactions in protein folding could be avoided and the system could be purely driven by hydrophobic interactions.

CHAPTER V

MODULATING LIGAND-RECEPTOR BINDING ON SUPPORTED LIPID BILAYER BY PHASE TRANSITIONS OF ELASTIN-LIKE POLYPEPTIDES

5.1. Synopsis

Elastin-like polypePtides (ELPs) exhibit reversible phase changes when the ambient temperature is above lower critical solution temperature (LCST). ELPs undergo a phase transition process in which the conformation switches from a random coil state to a compact globule state in response to a change in ionic strength or temperature. This property is utilized in this article to modulate ligand-receptor binding on solid supported lipid bilayers (SLBs). The ELPs were conjugated on the surface of SLBs as a nanoscale protein filter. The conformation of ELPs can be modulated by ionic strength of buffer solution or ambient temperature. These ELPs conjugated to the SLBs platform showed the ability to block IgG binding to biotin conjugated on the SLBs when the ELPs were in the extended coil state and opened access for protein to access biotin when in compact globule ELPs conformation.

5.2. Introduction

Microfluidics are widely utilized in the field of biosensing[11,76-77,152-153] due to the advantage of rapid analysis and small sample consumption.[154] On the other hand, biologic samples always contain a complex matrix and might affect sensing. Therefore, sometimes preanalysis steps are required. On-chip separation[155] is one method to deal with complex matrices. Fabricating multifunctional chips including separation and

detection not only costs more but also increases the possibility of failure. Also, the analysis process becomes tedious and lengthy with multiple sensing steps. A platform is needed with few steps to screen ligand-receptor interactions selectively.

Solid supported lipid bilayers (SLBs) are used in analytical system to study biological membrane properties[75] such as ligand-receptor binding[76-77] and interactions between lipids and protein.[78-80] The membranes possess two-dimensional fluidity similar to cell membranes, in that ligands on the surface can move along the surface and bind to a single protein with multiple binding sites.[156]

Previously in our group, a solid supported lipid bilayer microfluidic platform made with lipopolymer, poly(ethylene glycol)[11] (PEG) was made so that the conformation of PEG can be controlled by its density on the bilayers surface. At lower density, the PEG is in mushroom conformation so the IgG in the bulk solution can access the biotin conjugated on the surface. When the density of PEG is higher, the PEG undergoes a mushroom-to-brush transition and the access of IgG to biotin will be blocked. Herein, an advanced design is presented where the conformation of polymer on SLBs can be controlled in situ on the surface without altering the surface polymer density. Stimuli-responsive polymers have been used to control protein-ligand recognition. By changing the conformation of the polymer adjacent to binding site, binding events can be modulated.[12-14] The same concept was utilized here with the used of elastin-like polypeptides (ELPs) conjugated on the solid supported lipid bilayers as shown in Figure 5.1.

ELPs are biopolymers consisting of a repetitive pentapeptide unit, Val-Pro-Gly-Xaa-Gly. The guest residue, Xaa, can be any amino acid but not Pro. The ELPs undergo an inverse temperature transition[19-26] when the solution temperature become higher than a critical temperature called lower critical solution temperature (LCST). The conformation of the ELP is in a random disordered coil state in lower temperature and is fully hydrated. As the temperature goes above the LCST, the ELPs become compact globules and the solution turns cloudy. The conformation of ELPs on the surface can be changed by ionic strength or by temperature to s modulate ligand-receptor binding on the surface. The ELP utilized here is ELP[V_2I_7E]120 which means there are 120 of the pentaopeptides and Val, Ile and Glu where the guest residues at fourth position in a 2:7:1 ratio. The negatively charged Glu employed here is to prevent the ELPs from aggregation on the SLBs while in the extended conformation to achieve maximum filtration ability and also to prevent protein from absorbing on the ELP layer.

5.3.Experimental

Materials. POPC (1-Palmitoyl-2-Oleoyl-*sn*-Glycero-3-Phosphocloline), biotin-cap-PE (1,2-Dipalmitoyl-*sn*-Glycero-3-Phosphoethanolamine-*N*-(cap biotinyl) (Sodium Salt), Glutaryl PE (1,2-Dipalmoyl-*sn*-Glycero-3-phosphoetuanolamine- *N*-(Glutaryl) (Sodium Salt) were obtained from Avanti Polar Lipids (Alabaster, AL). Low-conductivity H_2O, produced from a NANOpure Ultrapure Water System (Barnstead, Dubuque, IA) with a minimum resistivity of 18 MΩ·cm, was used to prepare the

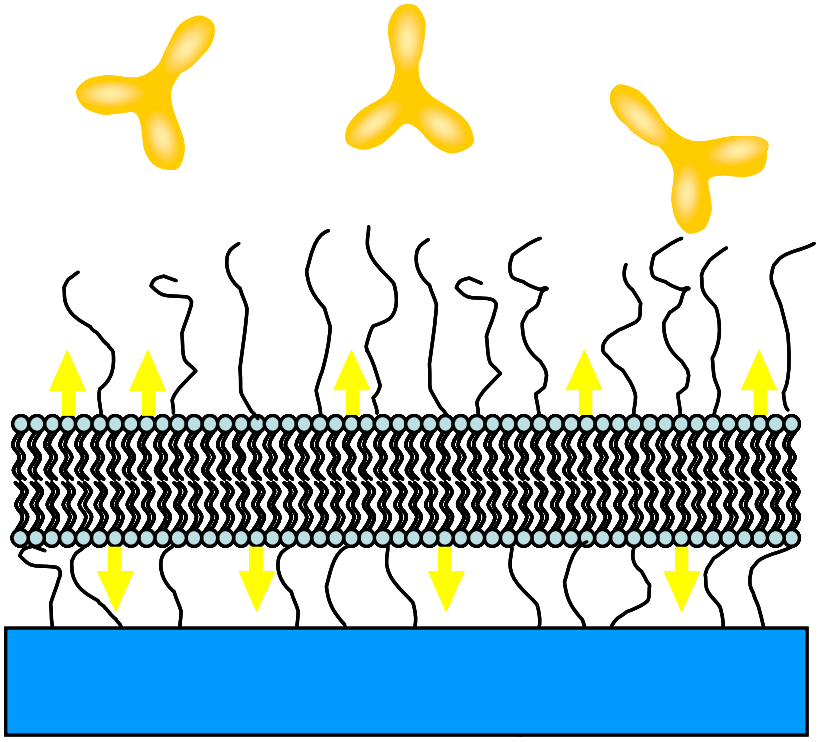

Figure 5.1. A schematic representation of ELPs blocking ligand-receptor binding on SLBs.

polymer and salt solutions. Sodium chloride was purchased from VWR (West Chester, PA). Sodium phosphate dibasic heptahydrate was obtained from Merck (Germany) and sodium phosphate was obtained from Sigma (St. Louis, MO). Anti-biotin IgG and anti-biotin IgG conjugated with Texas Red were purchased from Rockland (Gilbertville, PA). Alexa Fluor 594 protein labeling kit was purchased from Invitrogen (Eugene, OR). (1-Ethyl-3-[3-dimethylaminopropyl]carbodiimide hydrochloride) (EDC) and n-hydroxysuccinimide (NHS) were purchased from Thermo Fisher (Waltham, MA).

Small Unilamellar Vesicles. Small unilamellar vesicles (SUVs) were prepared as previous reported.[91-93] Briefly, lipids with the desired composition were mixed from stock solutions in chloroform. The solvent was then removed by a stream of nitrogen and further dried under vacuum for 4 h. The lipids were rehydrated after the solvent was removed completely by adding 10 mM phosphate buffer. The lipids were then subjected to 10 freeze-thaw cycles followed by 8 extrusions through two stacked polycarbonate membranes (Whatman) with 100 nm pores to produce vesicles of uniform size. The SUVs prepared by this procedure were 100 ± 10 nm in diameter determined by dynamic light scattering (Brookhaven Instruments 90Plus Particle size analyzer). The concentration of stock lipid solution was 2 mg/mL and kept at 4 ^{o}C before use.

Microfluidic Device. Microfluidic devices were made by soft lithographic methods.[157] The glass substrate (soda-lime glass slides, Corning, MA) was spin coated with a layer of photoresist (Shipley 1827) and exposed to UV light through photomask (Kodak technical pan film) with the desired image. The glass was then treated with developing solution and baked at 120 ^{o}C overnight. Buffered oxide etchant (BOE), a 1:6

ratio (v/v) of 48 % HF (EMD Chemicals Inc., Germany) and aqueous NH_4F (200 g in 300 mL purified water, Alfa Aesar, Ward Hill, MA), was used to etch glass. After the photoresist was removed by acetone, the patterned glass substrates were ready to be used as molds to make microfluidic devices. Next, a mixture of Sylgard silicon elastomer-184 and curing agent in a 10:1 ratio (w/w) was degassed under vacuum and poured over the glass substrates cured at 55 ^{o}C for overnight. A glass slide was cleaned in a boiling solution of ICN 7X (Costa mesa, CA) and purified water (1:4 (v/v)) for 30 min, then the glass slide was annealed in a kiln at 500 ^{o}C for 5 h before introducing to oxygen plasma then placed in oxygen plasma with cured PDMS for 10 seconds to bring the two pieces into contact.

ELPs Preparation. The ELP[V_2I_7E]120 was prepared as follows. The pET plasmids were constructed through recursive directional ligation.[57] The plasmids were expressed in BLR/DE3 *E. coli* in high growth TBdry media and ampicillin for 24 h. The ELPs were purified by sonicating the cells, then using inverse transition cycling (ITC) steps; two rounds of ITC were sufficient to remove impurities. The concentrations of the ELPs were determined by absorbance at 280 nm (ε =5690 M^{-1} cm^{-1}). The salts remaining in the solutions were removed by dialyzing against purified water (NANOpure Ultrapure Water System, Barnstead, Dubuque, IA) with a minimum resistivity of 18 MΩ· cm. The pure ELPs were then lyophilized and kept at – 80 °C.

Supported Lipid Bilayers. The ELPs were conjugated with vesicles by using a EDC/NHS coupling agent at 0 ^{o}C overnight before vesicle fusion step to form supported lipid bilayers (SLBs). The carboxylic acid groups on glutaryl PE react with primary

amine groups on the ELPs to form a stable ELP-lipid complex. Unreacted ELPs were removed by a centrifugal filter (YM-100 Centricon, Millipore, MA) under 1000g of spin rate for 20 min. The reacted vesicles were then introduced into freshly made microfluidic channels and incubated in the channels for 15 min. SLBs formed around the microfluidic channels spontaneously by vesicle fusion.[77] The excess vesicles were removed by injecting 10 mM phosphate buffer.

Epifluorescence and Total Internal Reflection Fluorescence Microscope. Epifluorescence images of Alexa Fluor 594 labeled IgG on SLBs were obatained using a Nikon E800 fluorescence microscope with a Roper Scientific MicroMax 1024B charge-coupled device (CCD) camera (Princeton Instruments). A total internal reflection fluorescence microscope[158] (TIRFM) was used to track the filtering ability with time. TIRFM was performed by using a 594 nm helium-neon laser (4 mW, Uniphase, Manteca, CA) passing through a dove prism with a line generator lens (BK7 for 20^{O}, Edmund Optics, Barrington, NJ) to create a uniform intensity profile across the microfluidic device.

5.4. Results

Density of ELPs on Surface. Tthe optimal density of ELPs was investigated first. The LCST of ELPs depends on the sequence, mole fraction and hydrophobicity of guest residues, chain length and concentration of ELPs. [58,132-134] In this case, the density of the ELPs on the surface is the main factor to determine the LCST, and hence, the filter ability of the solid supported lipid bilayers. Ideally, the coverage of ELPs on the surface

should have a LCST higher than room temperature. Thus, we can modulate the conformation of ELPs under ambient temperature. Also, the difference in surface coverage of the ELPs in different conformations should be as large as possible to show the on and off of filtering ability triggered either by temperature or ionic strength. The ELPs should cover as much area as possible when they are in random coils and also expose the maximum amount of ligands on the surface when they collapse into compact globules.

According to rough calculations from POPC size and the radius of ELPs measured by the particle size analyzer, 0.6 mol % of ELPs by number is needed to achieve the highest coverage on the surface. Due to the uncertainty of conjugation efficiency and uncertainty in compositions of the vesicles and the composition of the solid supported lipid bilayers, 0.3 mol % , 0.5 mol %, 1 mol %, 3 mol % and 5 mol % of glutaryl PE were tested.

After vesicle fusion and after excess vesicles were washed away, the solution containing Texas Red labeled IgG was introduced to the microfludic device and incubated for 15 minutes. After incubation, the channels were washed by phosphate buffer. The fluorescence intensity of channels revealed the ligand-receptor binding events on SLBs. The fluorescence intensity in the 0.3 mol % glutaryl PE was 23.4 % of the intensity in the control channel in which there were no ELPs on the SLBs. When the percentage of glutaryl PE was increased to 0.5 mol %, the relative intensity of ELPs conjugated SLBs channel decreased to 11.9 %, indicating the increase in ELPs on the surface covered more biotin, thus blocking more binding events. The lowest binding

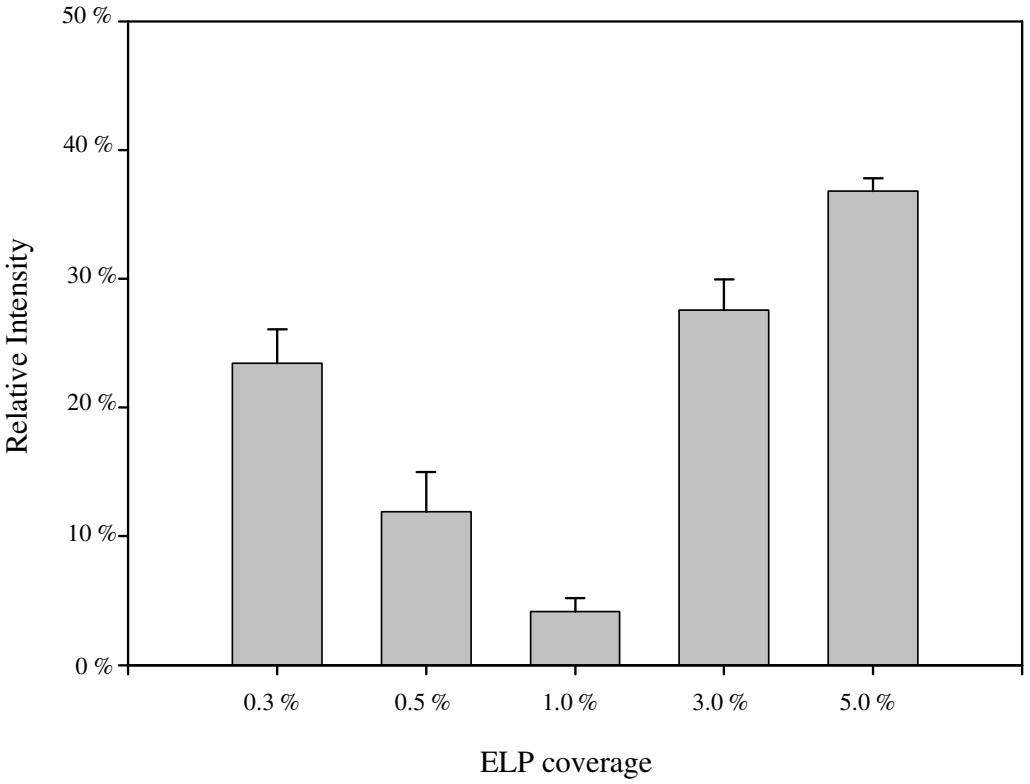

Figure 5.2. Relative intensity of ELP conjugated SLBs (1 mol % biotin-PE, and POPC). The fluorescence data was acquired after the bilayers were exposed to Texas Red labeled IgG in 500 mM NaCl and 10 mM phosphate buffer and compared to SBLs containing no ELPs.

events were observed from the 1 mol % glutaryl PE in the vesicle. The relative intensity showed 4.1 % as compare to the control channel. As the percentage of glutaryl PE further increased to 3 % and 5 %, the filter ability decreased; 27.6. % and 36.8 % relative intensity were observed from the 3 mol % and 5 mol % glutaryl PE vesicles. The results are shown in Figure 5.2.

This phenomenon is due to the fact that a high ELP density on the surface has a reduced LCST below ambient temperature that causes the collapse of ELPs. The globules formed after collapse reduces the coverage of ELPs on the surface, exposing biotin to IgG. 1 mol % of glutaryl PE showed the best filtration ability and is used in all other experiments.

If the density is too low on the surface, the coverage is too low and the filtration ability will be poor. On the other hand, if the density is too high, one possibility is that the LCST will be lower than room temperature. This will cause the conformations of the ELPs to shift from loose coils to compact globules. In that case, the filtration ability will also be poor because the coverage of ELPs on the surface will be reduced once the ELPs collapse.

Tunable Filtration Ability. The lipopolymer, poly(ethylene glycol) phosphatidylethanolamine (PEG-PE) incorporated SLBs have shown the ability to filter IgG by changing PEG density on the surface.[11] The concept of incorporating ELPs on the surface of the SLBs allows us to modulate the confirmation of ELPs in situ without changing the composition of bilayers. Therefore the filtration ability can be switch on and off.

In the “on” channel, the LCST of the ELPs immobilized on surface was depressed below ambient temperature by adding 1.5 M NaCl in the 10 mM phosphate buffer after the formation of the SLBs and washing. The ELPs on the SLBs in the “on” channel were allowed to interact with ions for 15 min. Then, IgG prepared with the same buffer (1.5 M NaCl in 10 mM phosphate buffer) was introduced into the channel and incubated for 10 min. In the “off” channel, only 10 mM phosphate buffer was used in the wash step, and IgG was prepared in 10 mM phosphate buffer without NaCl.

As shown in Figure 5.3, the fluorescence of Alexa Fluor 594 labeled IgG showed much stronger intensity in the “on” channel in which 1.5 mM NaCl was used to change the conformation of ELPs. The intensity in the “off” channel was only 0.78 % of the intensity of the “on” channel. Hence, the binding of IgG was 127.5 times greater in “on” channel which indicates that the biotin was covered by the ELPs when the ELPs were in extended coils and the access of IgG to the ligand was blocked. 1.5 M NaCl triggered collapse and exposed biotin to the IgG. On average, the fluorescence intensity ratio of the off/on channel was 3.7 ± 0.13 % indicating that binding was enhanced 26.9 times when the ELPs on the SLBs were in globules In a separate experiment, the fluorescence of “off” channel was monitored over 30 min by total internal reflection fluorescence microscope and the low florescence was maintained. A buffer containing 1.5 M NaCl was introduced into the channel and incubated for 15 min, then followed by an IgG solution prepared with 1.5 M NaCl in 10 mM phosphate buffer. The channel then showed a similar fluorescence compare to the “on” channel. This result indicated that the

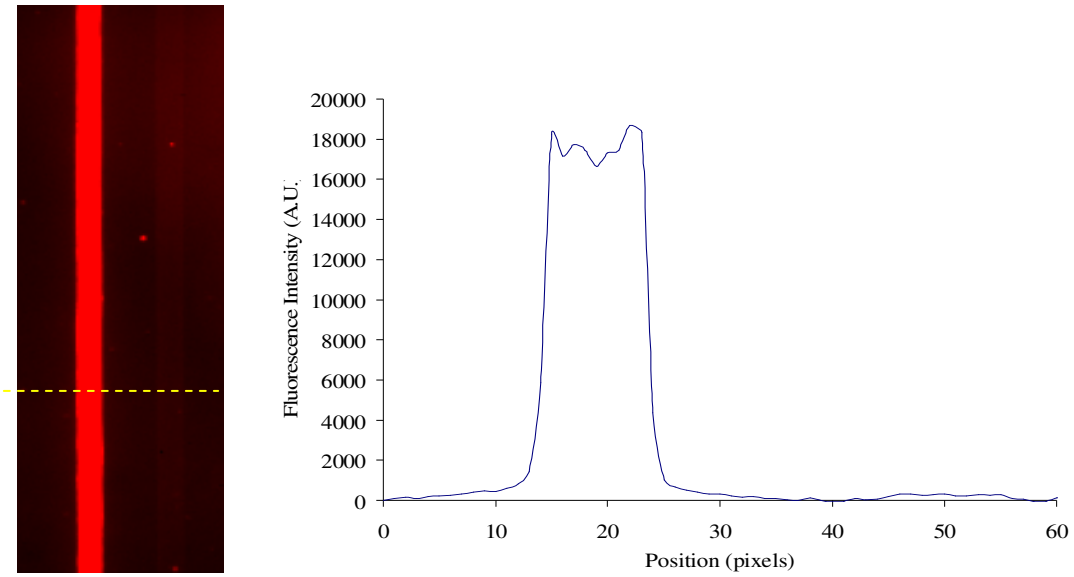

Figure 5.3. Left panel: Microfluidic device containing 1 mol % biotin-PE, 1 mol % glutaryl PE andd 98 mol % of POPC membrane conjugated with ELPs, and flowed with the 1.5 M NaCl, 10 mM phosphate buffer (left) and 10 mM phosphate buffer (right). Fluorescence micrograph was acquired after the bilayers were exposed to Alexa Fluor 594 lebeled IgG in 1.5 M NaCl, 10 mM phosphate buffer (left) and 10 mM phosphate buffer (right) then washed with buffers accordingly. Right panel: A line profile of fluorescence intensity (taken from yellow dashed line across the channels).

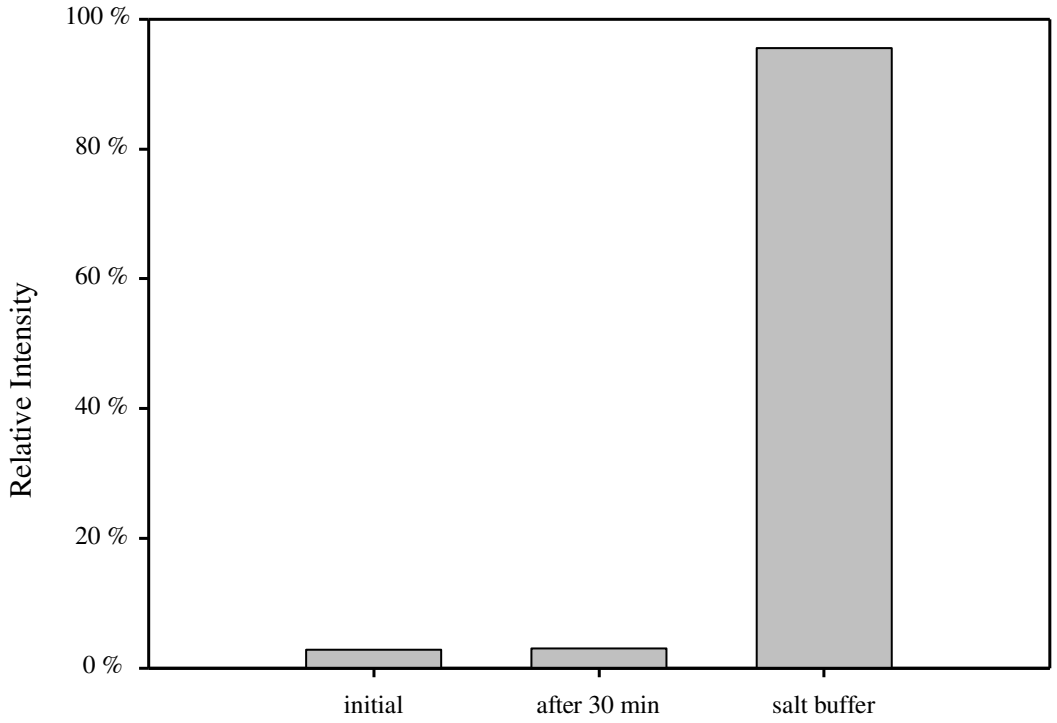

Figure 5.4. Relative intensity of ELP conjugated SLBs (1 mol % biotin-PE, 1 mol % glutaryl PE and 98 mol % of POPC). The fluorescence data was acquired after the bilayers were exposed to Texas Red labeled IgG and 10 mM phosphate buffer after 30 minutes and exposed to 1.5 M NaCl and 10 mM phosphate buffer containing Texas Red labeled IgG.

conformation of the ELPs on the SLBs could be changed and the filter can be turnED off. This result was showed in Figure 5.4.

Temperature Triggered Filtration Ability. The conformation of the the ELPs can also be controlled by temperature changes. A temperature gradient device[44-47] was utilized to provide different temperatures for different channels. Briefly, two brass tubes (1/8 in. wide, K&S Engineering, Chicago, IL) were placed parallel to each other. A hot fluid was circulated inside one tube while a cold fluid was circulated inside the other, creating a linear temperature gradient in between the two brass tubes. The microfluidic device was placed that the channels were parallel to the temperature gradient to create different temperatures in the different channels.

The temperature of the hot tube was set to be 60 ℃ and the tube was set to be 0 ℃. According to previous studies of IgG thermal stability, this temperature is not high enough to cause denaturation.[159] Three well separated channels were used to obtain a large temperature difference. The microfluidic channel at the highest temperature showed the strongest fluorescence due to the fact that ELPs are compact globules at high temperature, and expose the biotin on the surface for IgG binding. The fluorescence intensity of the channel in the middle showed a relatively weaker intensity, indicating that the biotin on the SLBs was only partially covered by the ELPs since the ELPs should be either compact globules or extended coils. The cold channel showed the weakest fluorescence intensity and therefore the lowest binding indicating the coil state of the ELPs covered biotin and blocked the access of IgG.

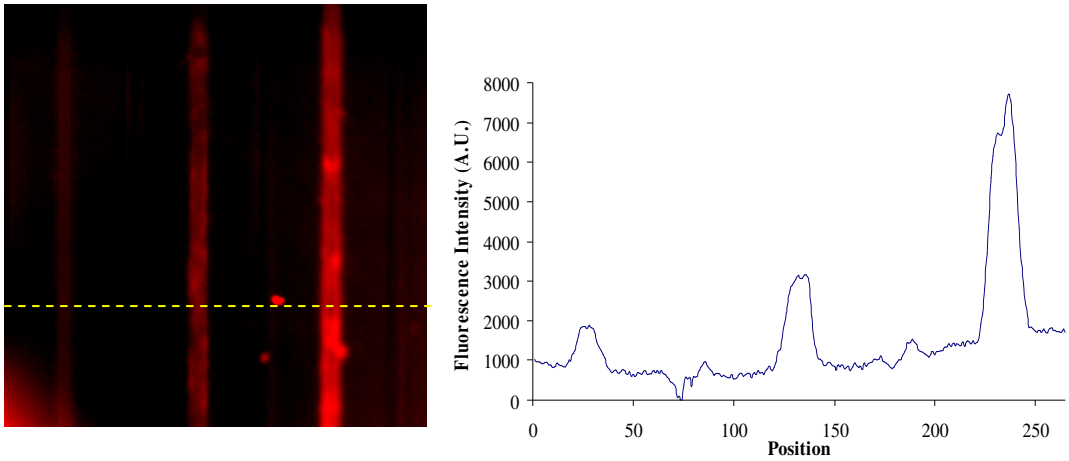

Figure 5.5. Left panel: Microfluidic device containing 1 mol % biotin-PE, 1 mol % glutaryl PE and 98 mol % of POPC membrane conjugated with ELPs and flow with 10 mM phosphate buffer. The microfluidic device was placed on a temperature gradient device with the hot source on the right and cold sink on the left. The fluorescence micrograph was acquired after the bilayers were exposed to Alexa Fluor 594 labeled IgG in 10 mM phosphate buffer. Right panel: A line profile of the fluorescence intensity (taken from yellow dashed line across the channels).

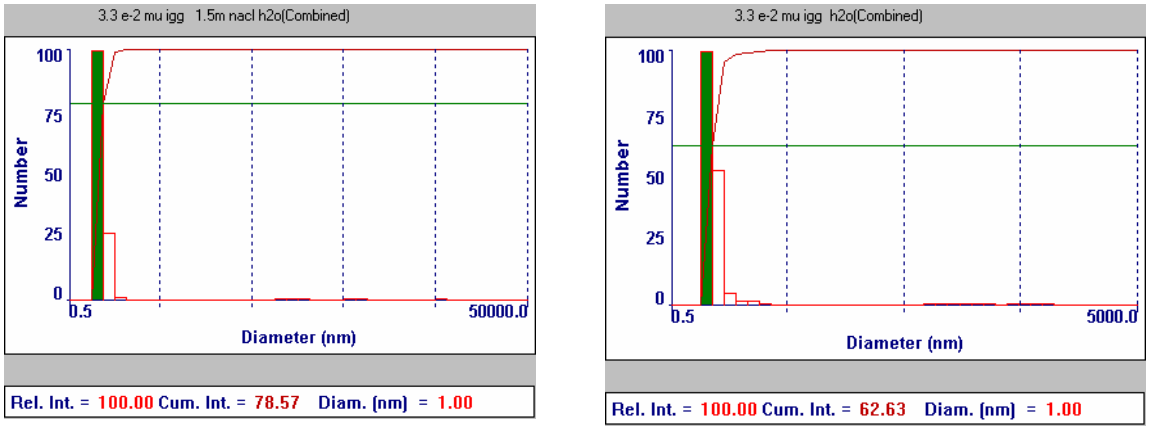

Figure 5.6. The size distribution of IgG measured by a particle size analyzer did not show a difference in the presence of 1.5 M NaCl (left panel), indicating the protein did not aggregate under the “on” condition.

The ratio of the three channels was 1:1.6:7.3. The filtration ability in this experiment is not as good as the ionic strength modulated one. One reason is that quantum efficiency of the dye is lower at high temperature. The other reason is that the binding of IgG to the ligands decreases as temperature increases.[160] Therefore, though the biotin was exposed to IgG , the binding events were depressed due to the high ambient temperature.

5.5. Discussion

The conformational change of the stimuli-responsive polymer was used to attach proteins in the vicinity of binding sites and to manipulate binding of protein.[12-14] This method typically requires a genetically engineered reactive site on the protein close to the binding site. No genetically engineered protein is needed using this method. Similar control over binding events can be achieved by incorporating ligands in the SBLs (for example, using biotinlated lipids) and conjugating stimuli-responsive polymer to lipids possessing reactive groups. Our approach requires less work and time. The in situ tunable filtration capacity of the ELP modified SLBs allows us to control and manipulate ligand-receptor binding in a simple, general fashion without having to design a reactive site near the binding site on the protein.

The optimal SLBs are prepared by using 1 mol % of glutaryl PE in the vesicle then reacting them with the ELPs for 24 h at 0 ^{o}C. This composition showed the best filtration ability under ambient temperature. The filtration ability can be turned off by using buffers containing salts. Base on the size measure by particle size analyzer, 0.6

mol % of the ELPs on the surface should be enough to cover all the ligand on the SBLs, however the conformation of the ELPs on the surface might not be the same as in bulk solutions. Therefore, the radius of gyration may be smaller and requiring larger numbers of ELPs. Furthermore, the conjugation reaction might not be 100 % efficient; therefore, almost twice the amount of ELPs may be needed before to the comparison to the theoretic calculations is reasonable.

Both temperature and ionic strength can modulate the conformation of the ELPs on the SLBs as shown in the previous section. The idea is to either increase the temperature above the LCST of the ELPs or to depress the LCST of the ELPs on the SLBs lower than the ambient temperature. Since the LSCT of the ELPs on the SLBs is determined by the coverage of ELPs, the guest residue composition, and chain length of ELPs, an optimal composition can be found to fit over a wide range of temperatures. A combination of different ELPs can be employed to tune the filtration ability.

As shown in Figure 5.6. the size distributions of IgG do not change in the presence of 1.5 M NaCl, indicating that there is no aggregation of protein during the "on" state and that the stronger signal in the channel is from more binding events, not from protein aggregation.

The advantage of employing ELPs instead of PEG on the SLBs is that the conformation of the ELPs can be modulated by either temperature or buffer composition in situ without having to alter the composition of the SLBs. There are many variables such as chain length, guest residue, and concentration which can be utilized depending

on the system requirements. The simple reaction of the primary amine of the ELPs and the carboxylic group on the lipid makes the conjugation easy and efficiency.

5.6 Conclusions

We developed a novel platform to modulate ligand-receptor binding on supported lipid bilayers using the phase transition of elastin-like polypeptides. The extended ELPs on the SLBs block the binding events. This filter can be turned on and off by changing ionic strength or temperature. Though the assay presented here was optimized for filtering IgG, this methodology is general and can be applied to other systems. The composition, length and density of ELPs on the surface could be optimized to filter different proteins.

CHAPTER VI

CONCLUSIONS

There are three main goals achieved in this dissertation. First, a novel temperature jump microfluidic system is established and showed the ability to measure of kinetics of PNIPAM collapse with different salts. Second,the application of this temperature jump microfluidic system is shown; a series of wild type ELPs with varies chain length are studied and the different contributions from backbone of ELPs, inter- and intramolecular hydrophobic interactions are studied separately. The third part is utilizing the phase transition property of ELPs; the ELPs conjugated SBLs shows the potential to modulate ligand-receptor binding by controlling the conformations of the ELPs in situ.

The novel temperature jump microfluidics provides a new way to study the phase transition kinetics that involved multiple chain aggregation. Some neurodegenerative diseases such as Alzheimer's disease, Parkinson's disease, and Huntington's disease are known to have molecular mechanisms involved protein aggregations. More research on the property of protein aggregation may provide more information about those diseases and may give more clues about the treatment. Furthermore, the study of biopolymers like PNIPAM and ELPs which have an inverse temperature transition[19,134,161-164] (which means the order increases both intermolecularly and intramolecularly on raising temperature) provides a similar system to the protein folding from the cold denaturation.

With proper design, this temperature jump microfudic system can be utilized to study the kinetic of ligand-receptor binding or the kinetics of protein folding, by labeling

ligand and receptor with fluorescence resonance energy transfer (FRET) pair or labeling at proper position in the protein sequence. Different pattern of microfuidics can be employed like Y shape channels to mix the sample with desired reagent before entering the temperature jump spot. Moreover, if this system is coupled with the temperature gradient system and multiple parallel channels are used; multiple temperature jumps with single run might be achieved to study the kinetics under different temperatures.

The study of the chain length effects on the phase transition of ELPs shows that the kinetics is mostly driven by the intermolecular hydrophobic interactions. Thought the thermodynamic parameters obtained from kinetic measurements are one order of magnitude greater than the values of the protein folding, the values related to single ELPs chain such as intramolecular hydrophobic interactions and backbone contributions fall into the same order as the protein folding values. This indicates the major difference between protein folding and ELPs collapse are intermolecular interactions while the intramolecular interactions are similar, at least in terns of energy scale. Further study might be done by employing ELPs with charged guest residue to see the polar side chain effects. The advantage of ELPs is it is easy to synthesis ELPs with other guest residues if needed.

The applications of ELPs on SLBs show the ability of ELPs to modulate the binding events on the bilayer surface. More complicated system can be done in the future, for example; a mixture of ELPs with different guest residues or different chain lengths can be used to create an ELPs covered surface with multiple LCSTs. This way, a multiple steps filtration might be achieved. Gradually changing the buffer compositions

or ambient temperatures might partially trigger the conformational change of ELPs on the surface and this might lead to partially expose the ligand on the bilayer surface and allow different receptor binding step by step.

REFERENCES

(1) Chan, H. S.; Dill, K. A. *Phys. Today* **1993**, *46*, 24-32.

(2) Pain, R. H. *Mechanisms of Protein Folding, 2nd ed.*; Oxford University Press, New York, NY, 2000.

(3) Onuchic, J. N.; Wolynes, P. G. *Curr Opin in Struct, Biol,* **2004**, *14*, 70-75.

(4) Matthews, C. R. *Annu. Rev. Biochem.* **1993**, *62*, 653-683.

(5) Martin, S. R.; Esposito, V.; Rios, P. D. L.; Pastore, A.; Temussi, P. A. *J. Am. Chem. Soc* **2008**, 130, 9963-9970.

(6) Williams, C.; Brochard, F.; Frisch, H. L. *Annu. Rev. Phys. Chem.* **1981**, *32*, 433-451.

(7) Chu, B.; Ying, Q.; Grosberg, A. Y. *Macromolecules* **1995**, *28*, 180-189.

(8) Yu, J.; Wang, Z.; Chu, B. *Macromolecules* **1992**, *25*, 1618-1620.

(9) Chu, B.; Ying, Q. *Macromolecules* **1996**, *25*, 1824-1826.

(10) Eyring, H. *J. of Chem. Phys.* **1935**, *3*, 107-115.

(11) Albertorio, F.; Daniel, S.; Cremer, P. S. *J. Am. Chem. Soc.* **2006**, *128*, 7168-7169.

(12) Stayton, P. S.; Shimoboji, T.; Long, C.; Chilkoti, A.; Chen, G.; Harris, J. M.; Hoffman, A. S. *Nature* **1995**, *378*, 472-474.

(13) Ding, Z.; Fong, R. B.; Long, C. J.; Stayton, P. S.; Hoffman, A. S. *Nature* **2001**, *411*, 59-62.

(14) Bulmus, V.; Ding, Z.; Long, C. J.; Stayton, P. S.; Hoffman, A. S.

Bioconjugate Chemistry **2000**, *11*, 78-83.

(15) Annaka, M.; Yahiro, C.; Nagase, K.; Kikuchi, A.; Okano, T. *Polymer* **2007**, *48*, 5713-5720.

(16) Gunari, N.; Balazs, A. C.; Walker, G. C. *J. Am. Chem. Soc.* **2007**, *129*, 10046-10047.

(17) Sun, S. T.; Nishio, I.; Swislow, G.; Tanaka, T. *J. Chem. Phys.* **1980**, *73*, 5971- 5975.

(18) Nakata, M. *Phys. Rev. E* **1995**, *51*, 5770-5775.

(19) Urry, D. W. *Journal of Protein Chemistry* **1988**, *7*, 1-34.

(20) Urry, D. W. *J. Phys. Chem. B* **1997**, *101*, 11007-11028.

(21) Cho, Y.; Zhang, Y.; Christensen, T.; Sagle, L. B.; Chilkoti, A.; Cremer, P. S. *J. Phys. Chem. B* **2008**, *112*, 13765-13771.

(22) Reguera, J.; Lagarn, J. M.; Alonso, M.; Reboto, V.; Calvo, B.; Rodrguez-Cabello, J. C. *Macromolecules* **2003**, *36*, 8470-8476.

(23) Rodrguez-Cabello, J. C.; Reguera, J.; Alonso, M.; Parker, T. M.; McPherson, D. T.; Urry, D. W. *Chemical Physics Letters* **2004**, *388*, 127-131.

(24) Meyer, D. E.; Chilkoti, A. *Nat. Biotechnol.* **1999**, *17*, 1112-1115.

(25) Trabbic-Carlson, K.; Meyer, D. E.; Liu, L.; Piervincenzi, R.; Nath, N.; LaBean, T.; Chilkoti, A. *Protein Eng., Des. Sel.* **2004**, *17*, 57-66.

(26) Reguera, J.; Urry, D. W.; Parker, T. M.; McPherson, D. T.; Rodrguez-Cabello, J. C. *Biomacromolecules* **2007**, *8*, 354-358.

(27) Sinha, J.; Dey, P. K.; Panda, T. *Appl. Microbiol. Biotechnol.* **2000**, *54*,

476-486.

(28) Hatti-Kaul, R. *Mol. Biotechnol.* **2001**, *19*, 269-277.

(29) Ban, T.; Shibata, M.; Kawaizumi, F.; Nii, S.; Takahashi, K. *J. Chromatogr., B* **2001**, *760*, 65-72.

(30) Johansson, H. O.; Persson, J.; Tjerneld, F. *Biotechnol. Bioeng.* **1999**, *66*, 247-257.

(31) Zhang, Y.; Trabbic-Carlson, K.; Albertorio, F.; Chilkoti, A.; Cremer, P. S. *Biomacromolecules* **2006**.

(32) Flamia, R.; Zhdan, P. A.; Martino, M.; Castle, J. E.; Tamburoo, A. M. *Biomacromolecules* **2004**, *5*, 1511-1518.

(33) Kumashiro, K. K.; Kurano, T. L.; Niemczura, W. P.; Martino, M.; Tamburoo, A. M. *Biopolymers* **2003**, *70*, 221-226.

(34) Ohgo, K.; Ashita, J.; Kumashiro, K. K.; Asakura, T. *Macromolecules* **2005**, *38*, 6038-6047.

(35) Ohgo, K.; Kurano, T. L.; Kumashiro, K. K.; Asakura, T. *Biomacromolecules* **2004**, *5*, 744-750.

(36) Schmidt, P.; Dybal, J.; Rodriguez-Cabello, J. C.; Reboto, V. *Biomacromolecules* **2005**, *6*, 697-706.

(37) Yao, X. L.; Hong, M. *J. Am. Chem. Soc.* **2004**, *126*, 4199-4210.

(38) Urry, D. W.; Long, M. M. *Crit. Rev. Biochem.* **1976**, *4*, 1-45.

(39) Nuhn, H.; Klok, H. A. *Biomacromolecules* **2008**, *9*, 2755-2763.

(40) Venkatachalam, C. M.; Urry, D. W. *Macromolecules* **1981**, *14*, 1225-1229.

(41) Martino, M.; Bavoso, A.; Guantieri, V.; Coviello, A.; Tamburoo, A. M. *J. Mol. Struct.* **2000**, *519*, 173-189.

(42) Ostuni, A.; Bochicchio, B.; Armentano, M. F.; Bisaccia, F.; Tamburoo, A. M. *Biophys. J.* **2007**, *93*, 3640-3651.

(43) Tamburoo, A. M.; Bochicchio, B.; Pepe, A. *Biochemistry* **2003**, *42*, 13347-13362.

(44) Zhang, Y.; Furyk, S.; Bergbreiter, D. E.; Cremer, P. S. *J. Am. Chem. Soc.* **2005**, *127*, 14505-14510.

(45) Mao, H.; Li, C.; Zhang, Y.; Bergbreiter, D. E.; Cremer, P. S. *J. Am. Chem. Soc.* **2003**, *125*, 2850-2851.

(46) Mao, H.; Holden, M. A.; You, M.; Cremer, P. S. *Anal. Chem.* **2002**, *74*, 5071-5075.

(47) Mao, H.; Yang, T.; Cremer, P. S. *J. Am. Chem. Soc* **2002**, *124*, 4432-4435.

(48) Wu, C.; Zhou, S. *Macromolecules* **1995**, *28*, 8381-8387.

(49) Qiu, X.; Li, M.; Kwan, C. M. S.; Wu, C. *J. of Pol. Sci. B* **1998**, *36*, 1501-1506.

(50) Picarra, S.; Duhamel, J.; Fedorov, A.; Martinho, J. M. G. J. *Phys. Chem. B* **2004**, *108*, 12009-12015.

(51) Picarra, S.; Relogio, P.; Afonso, C. A. M.; Martinho, J. M. G.; Farinha, J. P. S. *Macromolecules* **2003**, *36*, 8119-8129.

(52) Dill, K. A. *Biochemistry* **1990**, *29*, 7133-7155.

(53) Davidovic, M.; Mattea, C.; Qvist, J.; Halle, B. *J. Am. Chem. Soc* **2009**, *131*, 1025-1036.

(54) Pace, N. C.; Tanford, C. *Biochemistry* **1968**, *7*, 198-208.

(55) Wu, C.; Wang, X. *Phys. Rev. Lett.* **1998**, *80*, 4092-4094.

(56) Privalov, P. L.; Griko, Y. V.; Venyaminov, S. Y.; Kutyshenko, V. P. *J. Mol. Biol.* **1986**, *190*, 487-498.

(57) Meyer, D. E.; Chilkoti, A. *Biomacromolecules* **2002**, *3*, 357-367.

(58) Meyer, D. E.; Chilkoti, A. *Biomacromolecules* **2004**, *5*, 846-851.

(59) 2008 ANAT3231 Lecture 03 - Compartments and Membranes http://cellbiology.med.unsw.edu.au/units/science/lecture0803.htm 05/22/2010.

(60) Voet, D.; Voet, J. G.; Pratt, C. W. *Fundamentals of Biochemistry*; John Wiley & Sons. , 2006.

(61) Stoeckenius, W.; Engelman, D. M. *J. Cell Biol.* **1969**, *42*, 613-646.

(62) Singer, S. J.; Nicolson, G. L. *Science* **1972**, *175*, 720-773.

(63) Leito, A. M.; Cush, R. C.; Thompson, N. L. *Biophys. J.* **2003**, *85*, 3294-3302.

(64) Wetzwe, B.; Pum, D.; Sleytr, U. B. *J. Struct. Biol.* **1997**, *119*, 123-128.

(65) Brian, A. A.; McConnell, H. M. *Proc. Natl. Acad. Sci. U.S.A.* **1984**, *81*, 6159-6163.

(66) Tamm, L. K.; McConnell, H. M. *Biophys. J.* **1985**, *47*, 105-113.

(67) McConnell, H. M.; Watts, T. H.; Weis, R. M.; Brian, A. A. *Biochim. Biophys. Acta* **1986**, *864*, 95-106.

(68) Sackmann, E. *Science* **1996**, *271*, 43-48.

(69) Groves, T. J.; Boxer, S. G.; McConnell, H. M. *Proc. Natl. Acad. Sci. U.S.A.* **1997**, *94*, 13390-13395.

(70) Tamm, L. K. *Biochemistry* **1988**, *27*, 1450-1457.

(71) Cremer, P. S.; Boxer, S. G. *J. Phys. Chem. B* **1999**, *103*, 2554-2559.

(72) Cremer, P. S.; Groves, T. J.; Kung, L. A.; Boxer, S. G. *Langmuir* **1999**, *115*, 3893-3896.

(73) Groves, T. J.; Wulfing, C.; Boxer, S. G. *Biophys. J.* **1996**, *71*, 2716-2723.

(74) Groves, T. J.; Boxer, S. G. *Biophys. J.* **1995**, *69*, 1972-1975.

(75) Castellana, E. T.; Cremer, P. S. *Surface Science Reports* **2006**, 429-444.

(76) Jung, H. S.; Robison, A. D.; Cremer, P. S. *J. Am. Chem. Soc.* **2009**, *131*, 1006-1014.

(77) Jung, H. S.; Yang, T.; Lasagna, M. D.; Shi, J. J.; Reinhart, G. D.; Cremer, P. S. *Biophys. J.* **2008**, *94*, 3094-3103.

(78) Wagner, M. L.; Tamm, L. K. *Biophys. J.* **2001**, *81*, 266-275.

(79) Leidy, C.; Mouritsen, O. G.; Jørgensen, K.; G.H., P. *Biophys. J.* **2004**, *87*, 408-418.

(80) Merzlyakov, M.; Li, E.; Hristova, K. *Langmuir* **2006**, *22*, 1247-1253.

(81) Bayley, H.; Cremer, P. S. *Nature* **2001**, *413*, 226-230.

(82) Groves, T. J. *Curr. Opin, Drug Discov. Res* **2002**, *5*, 606-612.

(83) Daniel, S.; Diaz, A. J.; Martinez, K. M.; Bench, B. J.; Albertorio, F.; Cremer, P. S. *J. Am. Chem. Soc.* **2007**, *129*, 8072-8073.

(84) Suzuki, K.; Hosokawa, K.; Maeda, M. *J. Am. Chem. Soc.* **2008**, *130*, 1542-1543.

(85) Cunliffe, J. M.; NBaryla, N. E.; Lucy, C. A. *Anal. Chem.* **2002**, *74*, 776-783.

(86) Wang, C. Z.; Lucy, C. A. *Anal. Chem.* **2005**, *77*, 2015-2021.

(87) Bayerl, T. M.; Bloom, M. *Biophys. J.* **1990**, *58*, 357-362.

(88) Johnson, S. J.; Bayerl, T. M.; Mcdermott, D. C.; Adam, G. W.; Rennie,

A. R.; Thomas, R. K.; Sackmann, E. *Biophys. J.* **1991**, *59*, 289-294.

(89) Williams, L. M.; Evans, S. D.; Flynn, T. M.; Marsh, A.; Knowles, P. F.; Bushby, R. J.; Boden, N. *Langmuir* **1997**, *13*, 751-757.

(90) Koening, B. W.; Kruger, S.; Orts, W. J.; Majkrzak, C. F.; Berk, N. F.; Silverton, J. V.; Gawrisch, K. *Langmuir* **1996**, *12*, 1343-1350.

(91) Kalb, E.; Frey, S.; Tamm, L. K. *Biochim. Biophys. Acta* **1992**, *1103*, 307-316.

(92) Nollert, P.; Keifer, H.; Jahnig, F. *Biophys. J.* **1995**, *69*, 1447-1455.

(93) Albertorio, F.; Diaz, A. J.; Yang, T. L.; Chapa, V. A.; Kataoka, S.; Castellana, E. T.; Cremer, P. S. *Langmuir* **2005**, *21*, 7476-7482.

(94) Barenholtz, Y.; Litman, B. J.; Goll, J.; Tompson, T. E.; Carlson, F. D. *Biochemistry* **1977**, *16*, 2806-2810.

(95) Hamai, C.; Yang, T.; Kataoka, S.; Cremer, P. S.; Musser, S. M. *Biophys. J.* **2006**, *90*, 1241-1248.

(96) Groves, T. J.; Ulman, N.; Boxer, S. G. *Science* **1997**, *275*, 651-653.

(97) Zasadzinski, J. A. N.; Helm, C. A.; Longo, M. L.; Weisenhorn, A. L.; Gould, S. A. C.; Hansma, P. K. *Biophys. J.* **1991**, *59*, 755-760.

(98) Cremer, P. S.; Groves, T. J.; Ulman, N.; Boxer, S. G. *biophys. J.* **1998**, *74*, A311-A311.

(99) Cremer, P. S.; Yang, T. *J. Am. Chem. Soc.* **1999**, *121*, 8130-8131.

(100) Holden, M. A.; Kumar, S.; Castellanna, E. T.; Beskok, A.; Cremer, P. S. *Sensors and Actuators B* **2003**, *92*, 199-207.

(101) Axelrod, D.; Koppel, D. E.; Schlessinger, J.; Elson, E.; Web, W. W.

Biophys. J. **1976**, *16*, 1055-1069.

(102) Mammen, M.; Choi, S.-K.; Whiteside, G. M. *Angew. Chem. Int. Ed.* **1998**, *37*, 2754-2794.

(103) Bowden, N.; Brittain, S.; Evans, A. G.; Hutchinson, J. W.; Whiteside, G. M. *Nature* **1998**, *393*, 146-149.

(104) Xia, Y.; Whiteside, G. M. *Annu. Rev. Mater. Sci* **1998**, *28*, 153-184.

(105) Groves, T. J.; Boxer, S. G. *Acc. Chem. Res* **2002**, *35*, 149-157.

(106) Groves, T. J.; Mahal, L. K.; Bertozzi, C. R. *Langmuir* **2001**, *17*, 5129-5133.

(107) Holden, M. A. Ph.D. Dissertation, Texas A&M University, 2004.

(108) de Gennes, P. G. *Scaling Concepts in Polymer Physics*; Cornell University, Ithaca, NY, 1988.

(109) Athawale, M. A.; Goel, G.; Ghosh, T.; Truskett, T. M.; Garde, S. *PNAS* **2007**, *104*, 733-738.

(110) Baysal, B. M.; F.E., K. *Macromol. Theory Simul* **2003**, *12*, 627-646.

(111) Kuznetsov, Y. A.; Timoshenko, E. G.; Dawson, K. A. *J. Chem. Phys.* **1995**, *103*, 4807-4818.

(112) Wu, C.; Zhou, S. *Phys. Rev. Lett.* **1996**, *77*, 3053-3055.

(113) Wang, X.; Qiu, X.; Wu, C. *Macromolecules* **1998**, *31*, 2972-2976.

(114) Xu, J.; Zhu, Z.; Luo, S.; Wu, C.; Liu, S. *Phys. Rev. Lett.* **2006**, *96*, 278021-278024.

(115) Ross. D.; Gaitan, M. L., L.E. *Anal. Chem.* **2001**, *73*, 4117-4123.

(116) Tang, G.; Yan, D.; Yang, C.; Gong, H.; J.C., C.; Lam, Y. C.

Electrophoresis **2006**, *27*, 628-639.

(117) Schindler, T.; Schmid, F. X. *Biochemistry* **1996**, *35*, 16833-16842.

(118) Alexander, P.; Orban, J.; Bryan, P. *Biochemistry* **1992**, *31*, 7243-7248.

(119) Matagne, A.; Jamin, M.; Chung, E. W.; Robinson, C. V.; S.E., R.; Dobson, C. M. *J. Mol. Biol.* **2000**, *297*, 193-210.

(120) Tan, Y. J.; Oliveberg, M.; Fersht, A. *J. Mol. Biol.* **1996**, *264*, 377-389.

(121) Chen, B.; Baase, W. A.; Schellman, J. A. *Biochemistry* **1989**, *28*, 691-699.

(122) Wallace, M. I.; Ying, L.; Balasubramanian, S.; Klenerman *Proc. Natl. Acad. Sci. USA* **2001**, *98*, 5584-5589.

(123) Dobson, C. M.; Sali, A.; Karplus, M. *Angew. Chem. Int. Ed.* **1998**, *37*, 868-893.

(124) Frank, H. S.; Evans, M. W. *J. Chem. Phys.* **1945**, *13*, 507-532.

(125) Gill, S. J.; Dec, S. F. *J. Phys. Chem.* **1985**, *89*, 3758-3761.

(126) Makhatadze, G. I.; Privalov, P. L. *Protein Science* **1996**, *5*, 507-510.

(127) Makhatadze, G. I.; Privalov, P. L. *Biophysical Chemistry* **1994**, *51*, 291-309.

(128) Pegram, L. M.; Record, M. T. J. *J. Phys. Chem. B,* **2007**, *111*, 5411-5417.

(129) Broering, J. M.; Bommarius, A. S. *J. Phys. Chem. B,* **2005**, *109*, 20612-20619.

(130) Nishii, I.; Kataoka, M.; Tokunaga, F.; Goto, Y. *biochemistry* **1994**, *33*, 4903-3909.

(131) Kuroda, Y.; Kidokoro, S.; Wada, A. *J. Mol. Biol.* **1992**, *223*, 1139-1153.

(132) Urry, D. W.; Luan, C. H.; Parker, T. M.; Gowda, D. C.; Prasad, K. U.; Reid, M. C.; Safavy, A. *J. Am. Chem. Soc* **1991**, *113*, 4346-4348.

(133) Urry, D. W.; Trapane, T. L.; Prasad, K. U. *Biopolymers* **1985**, *24*, 2345-2356.

(134) Luan, C. H.; Harris, R. D.; Prasad, K. U.; Urry, D. W. *Biopolymers* **1990**, *29*, 1699-1706.

(135) Chang, C. Y.; Zhang, Y.; Cremer, P. S. *in preparation*.

(136) Schindler, T.; Schimid, F. X. *Biochemistry* **1996**, *35*, 16833-16842.

(137) Chen, B.; Schellman, J. A. *Biochemistry* **1989**, *28*, 685-691.

(138) Urry, D. W. *Methods in Enzymology* **1982**, *82*, 673-716.

(139) Yamaoka, T.; Tamura, T.; Seto, Y.; Tada, T.; Kunugi, S.; Tirrell, D. A. *Biomacromolecules* **2003**, *4*, 1680-1685.

(140) Privalov, P. L. *Adv. Protein Chem.* **1979**, *33*, 167-241.

(141) Baldwin, R. L. *Proc. Natl. Acad. Sci. USA* **1986**, *83*, 8069-8072.

(142) Baldwin, R. L.; Muller, N. *Proc. Natl. Acad. Sci. USA* **1992**, *89*, 7110-7113.

(143) Gill, S. J.; Nichols, N. F.; Wadso, I. *J. Chem. Thermodynamics* **1976**, *8*, 445-452.

(144) Murphy, K. P.; Privalov, P. L.; Gill, S. J. *Science* **1990**, *247*, 559-561.

(145) Doig, A. J.; Williams, D. H. *Biochemistry* **1992**, *31*, 9371-9375.

(146) Raffaele, R.; Colonna, G. *The Journal of Biological Chemistry* **1994**, *269*, 4047-4049.

(147) Spolar, R. S.; Livingstone, J. R.; Record Jr., T. M. *Biochemistry* **1992**, *31*, 3947-3955.

(148) Ben-Naim, A. *J. Phys. Chem.* **1991**, *95*, 1437-1444.

(149) Lee, B. *Proc. Natl. Acad. Sci. USA* **1991**, *88*, 5154-5158.

(150) Murphy, K. P.; Privalov, P. L.; Gill, S. J. *Science* **1990**, *247*, 559-561.

(151) Baldwin, R. L. *Proc. Natl. Acad. Sci. USA* **1986**, *83*, 8069-8072.

(152) Holman, H. N.; Miles, R.; Hao, Z.; Wozei, E.; Anderson, L. M.; Yang, H. *Anal. Chem.* **2009**, *81*, 8564-8570.

(153) Shi, J. J.; Yang, T.; Cremer, P. S. *Anal. Chem.* **2008**, *80*, 6078-6084.

(154) Jakeway, S. C.; de Mello, A. J. *Fresenius J. Anal. Chem.* **2000**, *366*, 525-539.

(155) Haeberle, S.; Zengerle, R. *Lab on a Chip* **2007**, *7*, 1094-1110.

(156) Jung, H. S.; Robison, A. D.; Cremer, P. S. *Journal of Structural Biology* **2009**, *168*, 90-94.

(157) Shi, J. J.; Yang, T.; Kataoka, M.; Zhang, Y.; Diaz, A. J.; Cremer, P. S. *J. Am. Chem. Soc* **2007**, *129*, 5954-5961.

(158) Axelrod, D.; Burghardt, T. P.; Thompson, N. L. *Annu. Rev. Biophys. Bioeng.* **1984**, *13*, 247-268.

(159) Vermeer, A. W. P.; Norde, W. *Biophys. J.* **2000**, *78*, 394-404.

(160) Lockshin, M. D.; Qamar, T.; Leva, R. A.; Best, M. P. *J. of Clinical Immunology* **1988**, *8*, 188-192.

(161) Li, B.; Alonso, D. O. V.; Daggett, V. *J. Mol. Biol.* **2001**, *305*, 581-591.

(162) Urry, D. W.; Trapane, T. L.; Iqbal, M.; Venkatachalam, C. M.; Prasad, K. U. *Biochemistry* **1985**, *24*, 5182-5189.

(163) Urry, D. W.; Gowda, D. C.; Parker, T. M.; Luan, C.-H.; Reid, M. C.; Harris, C. M.; Pattanaik, A.; Harris, R. D. *Biopolymers* **1992**, *32*, 1243-1250.

(164) Schreine, E.; Nicolini, C.; Ludolph, B.; Ravindra, R.; Otte, N.; Kohlmeyer, A.; Rousseau, R.; Winter, R.; Marx, D. *Phys. Rev. Lett.* **2004**, *92*, 148101-148104.

VITA

Name: Chin-Yuan Chang

Address: Department of Chemistry, 3255 TAMU, College Station, TX

Email Address: cychang@mail.chem.tamu.edu

Education:

Ph.D. in Chemistry
Texas A&M University
College Station, Texas
August, 2010
Adviser: Prof. Paul S. Cremer
Dissertation: Kinetics of an Inverse Temperature Transition Process and Its Application on Supported Lipid Bilayers

M.S. in Chemistry
National Taiwan University
Taipei, Taiwan,
June, 2004
Adviser: Prof Chuen-Ying Liu
Thesis: Polymeric Monolithic Column with Ligand Exchange Property for Capillary Electrochromatographic Separation of Cyclic and Linear Peptides.

B.S. in Chemistry
National Taiwan University
Taipei, Taiwan
June, 2002